(12) INTERNATIONAL APPLICATION PUBLISHED UNDER THE PATENT COOPERATION TREATY (PCT)

(19) World Intellectual Property Organization
International Bureau

(43) International Publication Date
28 December 2017 (28.12.2017)

WIPO | PCT

(10) International Publication Number
WO 2017/223092 A1

(51) International Patent Classification:
A61B 5/055 (2006.01) *A61K 51/00* (2006.01)
A61B 5/00 (2006.01) *A61M 5/00* (2006.01)
A61B 6/00 (2006.01) *G01N 33/68* (2006.01)
A61B 6/03 (2006.01)

(21) International Application Number:
PCT/US2017/038342

(22) International Filing Date:
20 June 2017 (20.06.2017)

(25) Filing Language: English

(26) Publication Language: English

(30) Priority Data:
62/352,869 21 June 2016 (21.06.2016) US
62/428,316 30 November 2016 (30.11.2016) US

(71) Applicant: **NEW YORK UNIVERSITY** [US/US]; 70 Washington Square South, New York, New York 10012 (US).

(72) Inventors: **DE LEON, Mony J.**; 70 Washington Square South, New York, New York 10012 (US). **RUSINEK, Henry**; 70 Washington Square South, New York, New York 10012 (US). **LI, Yi**; 70 Washington Square South, New York, New York 10012 (US).

(74) Agent: **KAPLUN, Oleg F.** et al.; 150 Broadway, Suite 702, New York, New York 10038 (US).

(81) Designated States *(unless otherwise indicated, for every kind of national protection available)*: AE, AG, AL, AM, AO, AT, AU, AZ, BA, BB, BG, BH, BN, BR, BW, BY, BZ, CA, CH, CL, CN, CO, CR, CU, CZ, DE, DJ, DK, DM, DO, DZ, EC, EE, EG, ES, FI, GB, GD, GE, GH, GM, GT, HN, HR, HU, ID, IL, IN, IR, IS, JO, JP, KE, KG, KH, KN, KP,

(54) Title: SYSTEM AND METHOD FOR IN VIVO DETECTION OF CEREBROSPINAL FLUID EGRESS

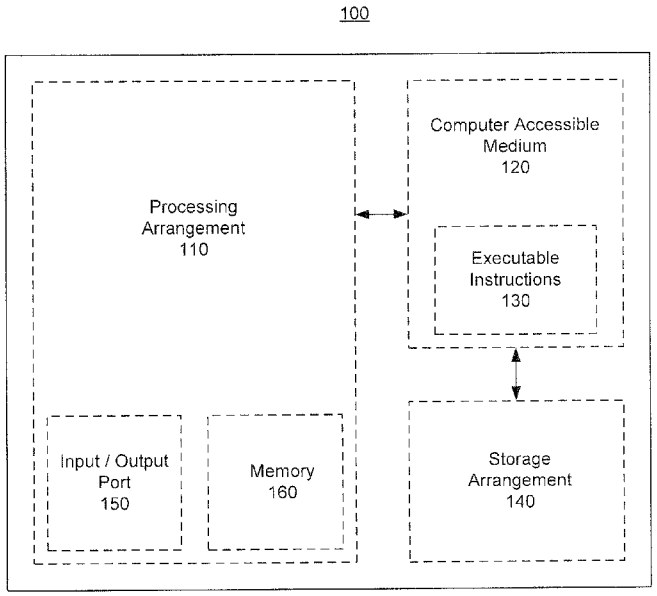

Fig. 1

(57) Abstract: Cerebrospinal fluid (CSF) egress in a patient may be detected in vivo by first intravenously administering a tracer capable of being taken up by brain tissue of the patient and subsequently clearing the brain tissue. The tracer may be detected using any suitable device in the patient's head, nasal and/or optic regions, and/or portion of or the entirety of the brain for a predetermined amount of time to obtain tracer data. The tracer data may be used to estimate a rate or a volume of CSF egress from the brain through a spinal fluid clearance pathway of the patient. The estimated rate or volume of CSF egress may be useful in providing the patient with a diagnosis for a neurological, inflammatory or cardiovascular disorder, e.g., Alzheimer's disease, traumatic brain injury, sleep disturbances, stroke and vascular disease, and brain conditions that cause an inflammatory response.

WO 2017/223092 A1

[Continued on next page]

KR, KW, KZ, LA, LC, LK, LR, LS, LU, LY, MA, MD, ME, MG, MK, MN, MW, MX, MY, MZ, NA, NG, NI, NO, NZ, OM, PA, PE, PG, PH, PL, PT, QA, RO, RS, RU, RW, SA, SC, SD, SE, SG, SK, SL, SM, ST, SV, SY, TH, TJ, TM, TN, TR, TT, TZ, UA, UG, US, UZ, VC, VN, ZA, ZM, ZW.

(84) Designated States *(unless otherwise indicated, for every kind of regional protection available)*: ARIPO (BW, GH, GM, KE, LR, LS, MW, MZ, NA, RW, SD, SL, ST, SZ, TZ, UG, ZM, ZW), Eurasian (AM, AZ, BY, KG, KZ, RU, TJ, TM), European (AL, AT, BE, BG, CH, CY, CZ, DE, DK, EE, ES, FI, FR, GB, GR, HR, HU, IE, IS, IT, LT, LU, LV, MC, MK, MT, NL, NO, PL, PT, RO, RS, SE, SI, SK, SM, TR), OAPI (BF, BJ, CF, CG, CI, CM, GA, GN, GQ, GW, KM, ML, MR, NE, SN, TD, TG).

Declarations under Rule 4.17:

— *as to applicant's entitlement to apply for and be granted a patent (Rule 4.17(ii))*

— *as to the applicant's entitlement to claim the priority of the earlier application (Rule 4.17(iii))*

Published:

— *with international search report (Art. 21(3))*

SYSTEM AND METHOD FOR *IN VIVO* DETECTION OF CEREBROSPINAL FLUID EGRESS

Inventor: Mony J. de Leon, Henry Rusinek, and Yi Li

PRIORITY CLAIM

[0001] This application claims priority to U.S. Provisional Patent Application Serial No. 62/352,869 filed June 21, 2016 and U.S. Provisional Patent Application Serial No. 62/428,316 filed November 30, 2016, entire contents of both provisional applications are hereby incorporated by reference herein.

GOVERNMENT FUNDING

[0002] This invention was made with government support under NIH/NIA Grant Nos. AG035137, AG032554, AG022374, and AG13616, AG12101, AG08051, NIH-HLB HL111724 and HL118624. The U.S. Government has certain rights in the invention.

BACKGROUND

[0003] There are two major extracellular fluid compartments associated with the central nervous system. One is the cerebrospinal fluid (CSF) that is mainly located in the cerebral ventricles and subarachnoid space. The other is the interstitial fluid (ISF) found in the spaces around brain cells.

SUMMARY OF THE INVENTION

[0004] In accordance with the foregoing objectives and others, one embodiment of the present invention provides a method for *in vivo* detection of cerebrospinal fluid (CSF) egress in a patient, particularly in a human. The method comprises a first step of intravenously administering a tracer capable of being taken up by brain tissue of the patient and subsequently clearing the brain tissue of the patient. The tracer may include, for example, tracers that are capable of binding to at least one of neurofibrillary tangles, neuropil threads, and beta-amyloid plaques in the brain tissue. Alternatively, tracers that do not bind to brain or extracranial sites are useful as they enable

clearance estimates to be made without having to account for tracer binding. In particular, the tracer may be a Positron Emission Tomography (PET) radiotracer, such as, for example, ^{18}F-THK5517, ^{11}C-PiB, ^{11}C-Cocaine, ^{18}F-THK5351, AV1451, MK6240, ^{11}C-Butanol, etc. Alternatively, the tracer may be a magnetic resonance imaging (MRI) contrast agent. Next, the method may comprise a step for continuously detecting the tracer in the patient's head and nasal region and/or at least a portion of the patient's brain for a predetermined amount of time to obtain tracer data. The tracer data may be obtained using a PET imaging device, in particular dynamic PET imaging. Alternatively, the tracer data may also be obtained using MRI imaging device. The tracer data may include any suitable type of data and may comprise at least one of time activity curves (TAC), areas under the curves (AUC), and standardized uptake value (SUV) images of the tracer over at least a portion of the predetermined amount of time. The method may further comprise the step of correlating the tracer data to a three-dimensional anatomical image of the patient's head, including nasal turbinate region, and other extracranial sites allowing the passage of CSF to the blood and the lymphatic system. The three-dimensional anatomical image may be a three-dimensional magnetic resonance imaging (MRI) image of the patient's head and nasal region. The method may further include a step for estimating a rate or a volume of CSF egress from a brain through a spinal fluid clearance pathway of the patient based the tracer data. The spinal fluid clearance pathway may comprise at least one of a cerebral ventricular system, a subarachnoid CSF compartment, a nasal turbinate, olfactory, optic or other cranial nerve. In another example, the tracer may be a non-binding tracer to brain tissue and estimates of CSF egress may be obtained directly from the brain. Lastly, the method may include a step for diagnosing a patient with a neurological, inflammatory or cardiovascular disorder based on the rate of CSF egress through the spinal fluid clearance system of the patient. The disorder may include, for example, Alzheimer's disease, traumatic brain injury, sleep disturbances, stroke and vascular disease, and brain conditions that cause an inflammatory response.

[0005] In another embodiment, an alternative method for *in vivo* detection of cerebrospinal fluid (CSF) egress in a patient is provided. The method comprises a first step of intravenously administering a tracer capable of being taken up by brain tissue of the patient and subsequently clearing the brain tissue of the patient. The tracer may include, for example, tracers that are capable of binding to at least one of neurofibrillary tangles, neuropil threads, and beta-amyloid plaques in the brain tissue, or tracers that do not bind to brain or other tissues. In particular, the tracer may

be a Positron Emission Tomography (PET) radiotracer, such as, for example, ^{18}F-THK5517, ^{11}C-PiB, ^{11}C-Cocaine, ^{18}F-THK5351, ^{18}F-MK6240, ^{11}C-Butanol, etc. Alternatively, the tracer may be a magnetic resonance imaging (MRI) contrast agent. Next, the method may comprise a step for continuously detecting the tracer in the patient's brain and extracranial head including the nasal region for a predetermined amount of time to obtain tracer data. The tracer data may be obtained using a PET imaging device, in particular dynamic PET imaging. Alternatively, the tracer data may also be obtained using MRI imaging device. The tracer data may include any suitable type of data and may comprise at least one of time activity curves (TAC), areas under the curves (AUC), and standardized uptake value (SUV) images of the tracer over at least a portion of the predetermined amount of time. The method may further comprise the step of identifying one or more voxels within an extra-cranial shell region of interest (ROI) of the patient, wherein the shell ROI is outside the brain and the subarachnoid space, and includes bone and soft tissue. The shell ROI may include at least one of dura, muscle, nasal turbinate and orbits. In some embodiments, the tracer data for each of the voxels are normalized by corresponding data for a cerebellar hemisphere gray matter of the patient. The method may further include a step for estimating a rate of CSF egress through at least one of the voxels within the shell ROI based on the tracer data. In one example, a first portion of the tracer data for the one or more voxels are temporally correlated to a second portion of the tracer data for lateral ventricles of the patient. In another example, a first portion of the tracer data for the one or more voxels is above a predetermined threshold value compared to the tracer data. In a further example, a first portion of the tracer data for the one or more voxels is correlated to an amount of tracer present in the patient's blood. Lastly, the method may include a step for diagnosing a patient with a neurological, inflammatory or cardiovascular disorder based on the rate of CSF egress through the spinal fluid clearance system of the patient. The disorder may include, for example, Alzheimer's disease, traumatic brain injury, sleep disturbances, stroke and vascular disease, and brain conditions that cause an inflammatory response or are associated with misfolded proteins. This procedure may also be used to establish risk in unaffected individuals such as elderly at risk for degenerative brain diseases.

[0006] In a further embodiment, a system is provided. The system may include an imaging device continuously gathering tracer data corresponding to uptake and clearance, within a brain of a patient, of a tracer intravenously administered to the patient, and a computing device comprising one or more processors and a set of instructions executing on the one or more processors. The set

of instructions are operable to: receive the tracer data from the imaging device, correlate the tracer data to a three-dimensional anatomical image of the patient's head, nasal region and/or brain, and estimating a rate or a volume of CSF egress from a brain through a spinal fluid clearance pathway of the patient based the tracer data.

[0007] In another embodiment, an alternative system is provided. The system may include an imaging device continuously gathering tracer data corresponding to uptake and clearance, within a brain of a patient, of a tracer intravenously administered to the patient, and a computing device comprising one or more processors and a set of instructions executing on the one or more processors. The set of instructions are operable to: receive the tracer data from the imaging device, identify one or more voxels within a shell region of interest (ROI) of the patient, wherein the shell ROI is outside the brain and the subarachnoid space, and includes bone and soft tissue, and estimating a rate of CSF egress through at least one of the voxels within the shell ROI based on the tracer data.

[0008] These and other aspects of the invention will become apparent to those skilled in the art after a reading of the following detailed description of the invention, including the figures and appended claims.

BRIEF DESCRIPTION OF THE FIGURES

[0009] Fig. 1 shows an exemplary computer system for performing method for *in vivo* detection of cerebrospinal fluid (CSF) egress.

[0010] Fig. 2 shows an exemplary embodiment of a method for *in vivo* detection of cerebrospinal fluid (CSF) egress.

[0011] Fig. 3 shows another exemplary embodiment of a method for *in vivo* detection of cerebrospinal fluid (CSF) egress.

[0012] Fig. 4 shows experimental data for percentage of voxels significantly correlated with ventricular CSF for subjects according to Example I.

[0013] Fig. 5 shows experimental normalized counts over a period of time for AUC for the correlated superior turbinate, arterial and venous blood, and brain according to Example I.

[0014] Fig. 6 shows experimental raw counts over a period of time for AUC for the correlated superior turbinate, arterial and venous blood, and brain according to Example I.

[0015] Fig. 7 shows experimental time activity curves (TAC) and AUC for the ventricular CSF and superior nasal turbinate in AD and control subjects according to Example I.

[0016] Fig. 8 shows experimental data in scattergrams for AD and control subjects for amyloid gray matter binding according to Example I.

[0017] Fig. 9 shows experimental data corresponding to tissue activity curves for F over a period of time according to Example I.

[0018] Fig. 10 shows experimental data corresponding to distribution of AUC for F over a period of time according to Example I.

[0019] Fig. 11 shows a table for a timing schedule for reconstructed PET image frames according to Example II.

[0020] Fig. 12 shows experimental data corresponding to a reference TAC for CSF and TAC for two sample shell voxels over a period of time according to Example II.

[0021] Fig. 13 shows experimental data correspond to percentage distribution of shell and nasal cavity voxels whose tau PET derived TAC are correlated with the ventricular CSF TAC according to Example II.

[0022] Fig. 14 shows experimental data corresponding to average tau tracer counts for subjects over a period of time according to Example II.

[0023] Fig. 15 shows experimental data corresponding to AUC of ventricle CSF clearance in patients with AD according to Example II.

[0024] Fig. 16 shows experimental data corresponding to rate of ventricle CSF clearance in patients with AD according to Example II.

[0025] Fig. 17 shows experimental data corresponding to positive superior turbinate voxels in patients with AD according to Example II.

[0026] Fig. 18 shows experimental data corresponding to ventricular tracer AUC over a period of time according to Example II

[0027] Fig. 19 shows experimental data corresponding to rate of ventricular tracer clearance over a period of time according to Example II.

[0028] Fig. 20 shows experimental data corresponding to ventricular tracer AUC over a period of time normalized to cerebrallar gray matter according to Example II.

[0029] Fig. 21 shows experimental data corresponding to ventricular tracer AUC over a period of time normalized to total brain parenchyma according to Example II.

DETAILED DESCRIPTION

[0030] A brain-wide paravascular CSF-ISF exchange mechanism has been shown in animal models to facilitate the clearance of waste products including soluble amyloid-β (Aβ) and tau protein. Studies in non-human species show a drainage pathway for subarachnoid CSF via olfactory nerves as they traverse the cribiform plate exchanging CSF at the nasal mucosa with lymphatic vessels for drainage via cervical lymph nodes. Drainage via the cribiform plate is rapid as radio labeled albumin Indian ink and paramagnetic contrast injected into the CSF reach the middle turbinates of the rodent nose within minutes. Other routes of CSF drainage have been identified along cranial and spinal nerves and most recently in the mouse via dural lymphatics. In humans it is believed that CSF can efflux directly back into blood via well-developed arachnoid granulations in the venous sinuses of brain and spinal cord which are not prominent in the rodent brain, however, the overall significance of this exit pathway is poorly characterized. While a CSF drainage pathway via the cribiform plate has been suggested in one human post mortem study, and hypothesized to be impaired in Alzheimer's Disease (AD) due to paravascular Aβ deposition, there had not previously been any *in vivo* evidence for a human cribiform drainage pathway. Using dynamic PET imaging with ^{18}F-THK5117, a tracer for tau pathology, the present application describes a CSF drainage pathway at the nasal turbinates in the human. Further, consistent with reported Aβ clearance deficits in AD, it is estimated that in AD a reduced volume of CSF cleared from the nasal turbinates and the lateral ventricles, with the amount of CSF cleared inversely associated with the magnitude of brain amyloid pathology, as determined by ^{11}C-PiB PET imaging.

[0031] Evidence that reduced CSF clearance is involved in the pathophysiology of Alzheimer's disease (AD) comes from primarily from rodent models. However, unlike rodents where predominant extracranial CSF egress is via the cribriform plate and olfactory nerves, human CSF clearance pathways are not well characterized. Using dynamic Positron Emission Tomography (PET) with ^{18}F-THK5117 a tracer for tau pathology, the ventricular CSF time activity may be used to identify extracranial CSF clearance sites.

[0032] In the rodent, CSF is primarily cleared along olfactory nerves that traverse the cribriform plate, draining into lymphatic vessels in the nasal mucosa. Rodent CSF clearance is rapid as radio- labeled albumin, Indian ink and paramagnetic contrast injected into the CSF reach the turbinates within minutes. Much less is known about the human CSF clearance anatomy.

Arachnoid granulations, arguably considered important human CSF egress sites, are not found in the rodent. The only evidence for a human nasal turbinate efflux pathway comes from post mortem studies. Using *in vivo* dynamic PET with ^{18}F-THK5117 and ^{11}C-PiB tracers in healthy elderly and demented subjects, ventricular CSF time activity curves (TAC) may be used to identify temporally correlated extracranial sites clearing CSF.

[0033] As discussed further below, Positron Emission Tomography (PET), typically employed to measure the uptake of radiotracers, was used to estimate the CSF clearance from brain after IV injection of THK5117 a tracer for tau protein. For each subject, a 3-D shell region surrounding the brain was created to identify voxels out of the brain whose time activity curves (TAC) were highly correlated ($r > .95$) with the ventricular CSF TAC. For all subjects, most densely correlated voxels were found in the superior nasal turbinates. The CSF identity of the correlated voxels was confirmed by matching their tracer AUC concentrations with those from ventricular CSF and showing they differed from brain and from arterial and venous blood. Region of interest sampling demonstrated anatomical specificity for the superior turbinate and ventricle tracer clearance for distinguishing between normal elderly and Alzheimer subjects. Further it was observed that the reduced CSF clearance in Alzheimer's disease is associated with an increased accumulation of amyloid using PET PIB imaging. These results suggest a functional CSF egress pathway through the human nasal turbinates, that may have value in neurological diseases with suspected impaired CSF clearance.

[0034] In one embodiment, an imaging device for detecting a tracer capable of being taken up by brain tissue of the patient and subsequent clearing the brain tissue of the patient may be provided. The tracer may be a tracer that binds to the brain tissue. Alternatively, the tracer may be a tracer that does not bind to the brain tissue. The imaging device may be any suitable imaging device for providing continuous imaging of a patient over any suitable predetermined period of time, *e.g.*, over a period of 40 mins, 50 mins, 80 mins, etc., in which CSF clearance and/or egress is to be observed. The imaging device may include, for example, Positron Emission Tomography (PET) imaging devices, in particular dynamic PET imaging devices, magnetic resonance image (MRI) imaging devices, etc. As would be understood by those having ordinary skill in the art, the imaging device may include any suitable imaging device that is capable of providing continuous and/or real-time imaging of CSF through brain tissue. The imaging device may further include, be operably connected to, or be in communication with any suitable processing arrangement for

analyzing the tracer data. Those skilled in the art will understand that the exemplary embodiments described herein may be implemented in any number of manners, including as a separate software module, as a combination of hardware and software, etc. For example, the exemplary analysis methods may be embodiment in one or more programs stored in a non-transitory storage medium and containing lines of code that, when compiled, may be executed by at least one of the plurality of processor cores or a separate processor. In some embodiments, a system comprising a plurality of processor cores and a set of instructions executing on the plurality of processor cores may be provided. The set of instructions may be operable to perform the exemplary methods discussed below.

[0035] For example, the exemplary analysis methods may be embodied in an exemplary system 100 as shown in Fig. 1. For example, an exemplary method described herein may be performed entirely or in part by a processing arrangement 110. Such processing/computing arrangement 110 may be, *e.g.*, entirely or a part of, or include, but not limited to, a computer/processor that can include, *e.g.*, one or more microprocessors, and use instructions stored on a computer-accessible medium (*e.g.*, RAM, ROM, hard drive, or other storage device). As shown in Figure 1, *e.g.*, a computer-accessible medium 120 (*e.g.*, as described herein, a storage device such as a hard disk, floppy disk, memory stick, CD-ROM, RAM, ROM, etc., or a collection thereof) can be provided (*e.g.*, in communication with the processing arrangement 110). The computer-accessible medium 120 may be a non-transitory computer-accessible medium. The computer-accessible medium 120 can contain executable instructions 130 thereon. In addition or alternatively, a storage arrangement 140 can be provided separately from the computer-accessible medium 120, which can provide the instructions to the processing arrangement 110 so as to configure the processing arrangement to execute certain exemplary procedures, processes and methods, as described herein, for example.

[0036] System 100 may also include a display or output device, an input device such as a key-board, mouse, touch screen or other input device, and may be connected to additional systems via a logical network. Many of the embodiments described herein may be practiced in a networked environment using logical connections to one or more remote computers having processors. Logical connections may include a local area network (LAN) and a wide area network (WAN) that are presented here by way of example and not limitation. Such networking environments are commonplace in office-wide or enterprise-wide computer networks, intranets and the Internet and

may use a wide variety of different communication protocols. Those skilled in the art can appreciate that such network computing environments can typically encompass many types of computer system configurations, including personal computers, hand-held devices, multi-processor systems, microprocessor-based or programmable consumer electronics, network PCs, minicomputers, mainframe computers, and the like. Embodiments of the invention may also be practiced in distributed computing environments where tasks are performed by local and remote processing devices that are linked (either by hardwired links, wireless links, or by a combination of hardwired or wireless links) through a communications network. In a distributed computing environment, program modules may be located in both local and remote memory storage devices.

[0037] Fig. 2 illustrates an exemplary method 200 for *in vivo* detection of cerebrospinal fluid (CSF) egress in a patient. In step 210, a subject for the analysis, in particular a human patient may be administered with a tracer for imaging analysis. The tracer may be administered to the patient by any suitable method, for example, by intravenous injection. The tracer may be any suitable radiotracer or contrast agent that is capable of being taken up by brain tissue of the patient and subsequently clearing the brain tissue of the patient. In particular, the tracer may be any suitable tracer that is suitable for crossing the blood-brain barrier. In some embodiments, the tracer may be capable of being taken up and cleared by brain tissue without substantial binding of the tracer to the brain tissue. In other embodiments, the tracer may be capable of binding to at least one of neurofibrillary tangles, neuropil threads, and beta-amyloid plaques in the brain tissue. In one example, the tracer may be capable of binding to a tau protein in the brain tissue. In another example, the tracer may be capable of binding to an amyloid in the brain tissue. In one exemplary embodiment, the tracer may be any suitable radiotracer, such as those suitable to be detected by Positron Emission Tomography (PET), such as, tau and amyloid tracers, such as, for example, ^{18}F-THK5517, ^{11}C-PiB, ^{18}F-THK5351, etc. In other examples, the PET tracer may be ^{11}C-Cocaine and/or ^{11}C-Butanol. In another example, the tracer may be a magnetic resonance imaging (MRI) contrast agent.

[0038] In step 220, tracer data may be obtained by detecting the migration of the tracer through the patient body, in particular, the patient's head and nasal region, and/or portions of or the entirety of the patient's brain. In particular, the tracer data may be detected by an imaging device in a continuous manner for any suitable predetermined period of time, *e.g.*, over a period of 40 mins, 50 mins, 80 mins, etc., in which CSF clearance and/or egress is to be observed. The imaging

device may include, for example, Positron Emission Tomography (PET) imaging devices, in particular, dynamic PET imaging devices, magnetic resonance image (MRI) imaging devices, etc. In one particular embodiment, the tracer data may be obtained by PET imaging, and more particularly by dynamic PET imaging. Alternatively, the tracer data may also be obtained using MRI imaging device. The tracer data may include any suitable type of data and may comprise at least one of time activity curves (TAC), areas under the curves (AUC), and standardized uptake value (SUV) images of the tracer over at least a portion of the predetermined amount of time.

[0039] In step 230, the tracer data may be correlated to a three-dimensional anatomical image of the patient's head and nasal region, and/or the portion of or the entirety of the patient's brain. The three-dimensional anatomical image may be a three-dimensional magnetic resonance imaging (MRI) image of the patient's head and nasal region, and/or a portion of or the entirety of the patient's brain. In some embodiments, the extracranial tracer data may be correlated to a three-dimensional anatomical image of an extracranial region of the patient's head and nasal region, while the tracer data for at least a portion of brain tissue may be correlated to a separate three-dimensional anatomical image of the corresponding portion of the brain. In a particular embodiment, the tracer data for the entirety of the patient's brain may be correlated to a three-dimensional anatomical image of the entirety of the patient's brain.

[0040] In step 240, the method may further include a step for estimating a rate or a volume of CSF egress from a brain through a spinal fluid clearance pathway of the patient based the tracer data. The spinal fluid clearance pathway may include any portion of the patient's spinal fluid clearance system where CSF is permitted to exit brain tissue of the patient. For example, spinal fluid clearance system may include a cerebral ventricular system, a subarachnoid CSF compartment, and/or a nasal turbinate (in particular, the superior nasal turbinate). The CSF egress pathway may also traverse the cribriform plate to the superior turbinate and to nasal cavity lymphatics. The estimated rates and/or volumes of CSF egress from the brain through the spinal fluid clearance system may be used to diagnose a patient with a neurological, inflammatory or cardiovascular disorder based on the rate of CSF egress through the spinal fluid clearance system of the patient. For example, patients having a reduced rate or volume of CSF egress may be indicative of a neurological, inflammatory or cardiovascular disorder. The disorder may be a disease with abnormal protein deposits (*e.g.*, misfolded brain proteins) such as, for example, Parkinson's disease, progressive supranuclear palsy, and Alzheimer's disease. Other disorders

may include, traumatic brain injury, sleep disturbances, stroke and vascular disease, brain conditions that cause an inflammatory response, etc. The rate and/or volume of CSF egress may also be indicative of intra-laminar tau distributions in lesion progression. Based on the estimated rates and/or volumes of CSF egress from the brain through the spinal fluid clearance system, a physician may provide treatment to improve the rate and/or volume of CSF egress in a patient, such as, for example, modification of sleep of the patient, etc. Such treatments to modify the rate and/or volume of CSF egress in a patient may impact (*e.g.*, reduce) the brain's burden of accumulated misfolded proteins, such as, for example, tau and amyloid proteins.

[0041] Fig. 3 illustrates another exemplary method 300 for *in vivo* detection of cerebrospinal fluid (CSF) egress in a patient. Steps 310 and 320 are substantially similar to step 210 and 220 as discussed above. In one embodiment, the tracer data for each of the voxels may be normalized by at least a portion or an entirety of the patient's brain. For example, the portion may include one or more of the lateral ventricle, neocortical gray and white matter, and cerebellar hemisphere gray matter of the patient. In some embodiments, the tracer data for each of the voxels are normalized by corresponding data for a cerebellar hemisphere gray matter of the patient. In step 330, one or more voxels within a shell region of interest (ROI) of the patient may be identified for further analysis. The shell ROI is an area outside the brain and the subarachnoid space of the patient, and includes the bone and soft tissue. In particular, the shell ROI may include at least one of dura, muscle, nasal turbinate and orbits.

[0042] The one or more voxels may be identified via any suitable way for identifying those voxels in which substantial amounts of the tracers pass through, or those voxels that temporally correspond to flow of CSF out of brain tissue. In some embodiments, the one or more voxels may be identified by any suitable quantitative model for clearance of the tracer into the CSF compartment (system). The one or more voxels may be identified using a kinetic model of CSF tau clearance. In other embodiments, the one or more voxels may be identified based on the rate of incorporation of tracer into the brain. In other embodiments, the one or more voxels may be identified based on the rate of removal of tracer from the brain, for example, dynamic PET imaging may be correlated to data obtained from periodic blood sampling. The blood sampling may be obtained from, for example, an internal carotid artery, or may be venous blood sampled at the junction of the superior sagittal and transverse sinus. In one example, a first portion of the tracer data for the one or more voxels may be temporally correlated to a second portion of the tracer data

for lateral ventricles of the patient. In another example, a first portion of the tracer data for the one or more voxels is above a predetermined threshold value compared to the tracer data. In a further example, a first portion of the tracer data for the one or more voxels is correlated to an amount of tracer present in the patient's blood.

[0043] In step 340, an estimate may be obtained for a rate or volume of CSF egress through at least one of the voxels within the shell ROI based on the tracer data. The estimated rates and/or volumes of CSF egress from the brain through the one or more voxels may be used to diagnose a patient with a neurological, inflammatory or cardiovascular disorder based on the rate of CSF egress through the spinal fluid clearance system of the patient. For example, patients having a reduced rate or volume of CSF egress may be indicative of a neurological, inflammatory or cardiovascular disorder, such as, for example, Alzheimer's disease, traumatic brain injury, sleep disturbances, stroke and vascular disease, and brain conditions that cause an inflammatory response. The rate and/or volume of CSF egress may also be indicative of intra-laminar tau distributions in lesion progression. Based on the estimated rates and/or volumes of CSF egress from the brain through the one or more voxels, a physician may provide treatment to improve the rate and/or volume of CSF egress in a patient, such as, for example, modification of sleep of the patient, etc.

EXAMPLE

Example I

METHODS

Participants and clinical procedures

[0044] 15 subjects were studied including 7 healthy elderly controls (4 males and 3 female, age 74.1±5.6, range 67-83 years, MMSE 28.6±1.6, Clinical Dementia Rating (CDR) of 0, education 14.6±2.2 years) and 8 with probable AD (2 female and 6 males, age 79.8±10.6, range 57-89 years, Mini-Mental State Examination (MMSE) 18.5±4.6, CDR of 2.0±0.8, education 12.1±2.7 years). Participants received standardized neuropsychological and clinical assessments, and a high resolution T1 weighted MRI scan. The AD diagnoses were made at a consensus conference according to the National Institute of Neurological and Communicative Disorders and Stroke/AD and Related Disorders Association criteria. AD patients were recruited from the memory clinic of Tohoku University Hospital. An ethics committee approved written informed consent was obtained from all participants or the legal care takers. All 15 subjects underwent two

dynamic acquisition PET exams (^{18}F-THK5117 and ^{11}C-PiB) except for 2 controls that did not complete ^{11}C-PiB PET imaging.

Image Acquisition and processing

[0045] PET acquisitions: The PET radiotracers were administered in two imaging sessions within 2 weeks. The radiotracer (18)F-labeled arylquinoline derivative 6-[(3-18F-fluoro-2-hydroxy)propoxy]-2-(4-methylaminophenyl)quinoline or THK-5117, was developed and validated for binding to neurofibrillary tangles and neuropil threads. The second radiotracer, Pittsburgh compound B (^{11}C-PiB), an analog of thioflavin T is validated biomarker for beta-amyloid plaques in brain tissue. Both tracers were prepared at the Cyclotron and Radioisotope Center of Tohoku University, and both have low molecular weight (<5KD) and both show rapid brain uptake and clearance. 185 mBq of ^{18}F-THK5117 and 296 mBq of ^{11}C-PiB were administered by IV bolus injection. PET data were acquired axially along the cantho-meatal plane in list mode continuously for 90 min. using an Eminence STARGATE PET scanner (Shimadzu, Kyoto, Japan). Another suitable PET imaging device may be the Eminence SET-3000GCT-X (Shimadzu Corp., Kyoto, Japan) scanner for measuring regional brain radioactivity. This scanner provides 99 sections with an axial field of view (FOV) of 26.0 cm. The spatial resolution was 3.45 mm in-plane and 3.72 mm full-width at half-maximum (FWHM) axially. The superior- inferior field of view for the PET scans encompassed the skull superiorly and inferiorly the foramen magnum and maxilla.

[0046] MRI acquisition: Each subject received a 3-D volumetric MRI study using a high-resolution T1-weighted SPGR gradient echo sequence that produced 110 gapless axial sections with 2.0mm voxel size (echo time/repetition time, 2.4/50 ms; flip angle 45°; acquisition matrix 256×256; 1 excitation; axial field of view 22 cm, with 110 slices with a thickness, 2.0 mm, (SIGNA 1.5 T magnet, General Electric, Milwaukee, WI). In all cases, the MRI field of view (FOV) covered the PET FOV. The MRI was used for regional tissue segmentation and to correct the PET for partial volume effects.

[0047] ***PET Image Workflow*:** The data for both tracers was decay corrected and standardized uptake value (SUV) images created by normalizing by injected dose and body weight. The SUV images were displayed with a 2.6 mm slice thickness and a 2x2 mm in plane voxel size. SPM12 default procedures using affine transformations were used for realignment of the dynamic PET frames and for coregistration of the T1 weighted MRI with the original PET data

(www.fil.ion.ucl.ac.uk/spm). The partial volume correction for the higher brain count contamination of lower count CSF signals was examined with a modified one tissue model. All results reported remained significant after the correction and the corrected results are presented in the appendix.

MRI Regional Segmentation and ROI's:

[0048] To test for the hypothesized nasal turbinate egress portal, using SPM12, a shell region of interest (ROI) was defined on MRI which included bone, and soft tissue (e.g. dura, muscle, nasal turbinates, and orbits) and excluded brain, subarachnoid CSF, and air. Hypothesis testing was done using anatomical ROIs drawn on MRI scans resliced to a standard plane and reformatted back to the coregistered PET scans to sample the PET in the original space. The ROIs included: the superior nasal turbinate, 4mm inferior to the cribiform plate, to minimize contamination with brain, with the anterior boundary at the crista galli (18 mm length, 14 mm width and 10mm depth); the middle nasal turbinate ROI inferior to the superior (34 mm length, 16 mm width and 18 mm depth); bilaterally the orbits and lateral pterygoid muscles (ROIs 12 mm length, 12 width and 6mm depth). Additional ROIs were determined for the ventricular CSF by shrinking the outer ependymal margin by 3 voxels to minimize contamination from brain tissue. Arterial blood was sampled from the PET images at the internal carotid artery and venous blood sampled the junction of the superior sagittal and transverse sinus. SPM12 was used to segment the gray matter of the cerebellar hemispheres. For all ROIs, time activity curves (TAC) and areas under the curves (AUC) were created and normalized by the corresponding measure from the cerebellar gray matter.

[0049] ***Estimations of PET tracer binding*:** Estimates of amyloid deposition and tau deposition were determined from the sum of the SUV 50-80 min time frames normalized by the cerebellar hemispheric gray matter SUV to form the SUV ratio (SUVR). SUVR values $\geq$ 1.5 were used to threshold tracer binding.

[0050] ***Mapping and validating tracer clearance*:** To identify and anatomically map CSF signals in the shell for each subject, the TAC of every shell voxel was correlated with the TAC from the ventricular CSF ROI. Correlations were determined from 3 minutes post injection to 80 min. resulting in voxel-wise correlations based on 28 time points for each subject. The data show that across all subjects, the percentage of turbinate voxels correlated with CSF reached a peak at r=.95. By comparison, for the total shell the percentages of significant voxels did not vary much with the magnitude of the correlation. Very similar distribution were observed for the normal and

AD groups examined separately Overall, a significantly lower percentage of shell voxels were correlated with "pure" CSF (see Figure 4). Figure 4 depicts for all subjects the percentage +/- SEM of voxels significantly correlated with ventricular CSF (r range .90-1.00) for the combined superior and middle turbinates and the total shell. In the first step, shell voxels whose signals correlated with CSF at $r \geq .95$ were mapped to the MRI. As the correlation between TAC does not reflect the absolute tracer concentration, in a second step, the AUC for the correlated superior turbinate voxels were compared with the AUC from blood, CSF and brain and the other ROIs. This was done for the 35-80 min period (a period when CSF and blood values approximate steady state and could be distinguished, see Figures 5 and 6). Figures 5 and 6 demonstrate over the 35-80min the normalize counts (Fig. 5 and the raw count TAC in Fig. 6). Specifically, the AUC of the superior turbinates and ventricular CSF do not differ, nor do the arterial and venous blood AUC differ from each other. However, the blood AUCs are significantly lower than either the CSF or the superior turbinates. The brain has a consistently greater AUC due to specific and non-specific tracer binding.

Statistical analysis:

[0051] All TAC, AUC, and SUV, data were normalized by the corresponding cerebellar hemisphere gray matter data. The principal data analyses were conducted using non-parametric tests and confirmed with parametric tests. Correlations were examined with Spearman and Pearson Product tests. Groups contrasts were made using Mann-Whitney U and T-tests. Within subject tests of anatomical specificity were examined with related samples Wilcoxon Signed Rank Tests and Paired t-tests. Following Bonferroni correction for multiple comparisons the p value $< .017$ was considered significant.

Hypotheses:

[0052] We tested four hypotheses: 1. Evidence for a cribiform plate CSF egress pathway would come from two sources: the superior nasal turbinates would consistently show across subjects and across shell ROIs a high density of voxels whose time course is closely associated with the ventricular CSF; and superior turbinate sites identified CSF portals would show tracer concentrations consistent with CSF and tracer concentrations differing from blood and brain; 2. AD patients relative to control show anatomically specific reduced CSF clearance as seen in both superior turbinates and ventricle; and 3. Superior turbinate and ventricular CSF clearance is inversely associated with brain amyloid deposition as estimated from PIB-PET.

RESULTS

[0053] In support of hypothesis 1, all subjects showed turbinate voxel TACs associated with the ventricular TAC. Moreover, the highest density of correlated shell voxels was in the superior turbinate ROI followed by middle turbinate, and with very little CSF signal in the muscle or orbital ROIs (see Table 1). Table 1 shows positive CSF correlated voxels by regions for all subjects.

Table 1.

	Superior turbinate	Middle turbinate	eye	muscle	shell
Number Voxels in ROI	315	1160	360	216	181621 (23086)
Number Positive Voxels (sd)	74.7 (61.7)	264.9 (194.4)	15.4 (13.2)	5.62 (5.08)	7139.0 (3520.8)
ROI Voxel density% (sd)	23.7 (20.1)	22.8 (15.9)	4.3(3.6)	2.6 (2.3)	3.9 (2.0)
AUC35-80	0.61(.09)	0.54(.09)	0.35(.28)	0.43(.25)	0.53(.06)

Data showed in mean(sd)

[0054] The superior turbinate ROI is 0.2% of the shell volume and contains 1.0% of the total shell correlations with CSF. Combined superior and middle turbinates account for 5% of the positive shell voxels. The data show that nearly 80% of the remaining counts are in the CSF structures including the subarachnoid space.

[0055] Further supporting the CSF origin of the turbinate signal, the AUC analyses showed that the superior turbinate AUC did not differ from the ventricular AUC, ($W=6.8$, $p>.05$). However, the superior turbinate AUC was lower than whole brain ($W=3.41$, $p<0.01$), but significantly higher than both arterial ($W=-2.56$, $p=0.01$) and venous blood ($W=-2.33$, $p<0.05$). The arterial and venous blood AUC's did not differ from each other ($W=.51$, $p>0.05$, see Figures 5 and 6). Overall, these data show that the superior turbinate signals that have a time course highly correlated with the CSF and tracer concentrations most consistent with CSF. We also observed that the superior turbinate signals were greater than those found in other the regions tested, specifically, the orbit ($W=-2.95$, $p<0.01$) and ptergoid muscle ($W=-2.27$, $p<0.05$) (table1). Further, the question of reduced blood flow as a potential confound with respect to interpreting the between region AUC was modeled and demonstrated to have a negligible effect on the AUC.

Areas under the time activity curves are not sensitive to changes in cerebral blood flow (CBF).

[0056] One possible interpretation of regional differences in area under the curve (AUC) is the CBF. To estimate the effect of regional perfusion rate *F* on AUC, representative datasets were simulated for a wide range of *F*. The simulation was governed by the kinetic model of a diffusible tracer in which the relation between the arterial input function $c_a(t)$ and the tissue response function c(t) is given by:

$$c'(t) = F\{c_a(t) - c(t)\} \qquad \text{Eq. 1}$$

where prime denotes the time derivative. The analytic solution of Eq.1 is:

$$c(t) = Fe^{-Ft}\int_0^t c_a(u)e^{Fu}\,du \qquad \text{Eq. 2.}$$

[0057] The arterial input was generated as the average of values extracted from all 15 patients after aligning the peaks. Fig. 9 shows the tissue activity curves for *F* varying in the range 35-60 ml/100g/min. Fig. 10 shows the corresponding distribution of AUC for the time period 10-35 min after injection, demonstrating negligible effect of F.

[0058] Comparing AD with control subjects confirmed the anatomic specificity of the superior turbinate among shell regions (see Figure 7 and Table 2). Table 2 shows group differences for positive voxel number, density, AUC and cleared tracer load. Figure 7 shows by group the 3min. to 80min. TAC for the ventricular CSF AUC and the superior nasal turbinate load (top row). The data are expressed as normalized by the cerebellar gray matter (bottom row). Both the corrected ventricular ($U=6$, $p<0.01$) and the turbinate concentrations ($U=8$, $p=0.02$) and the uncorrected data are significantly lower in AD.

Table 2.

	Positive Voxel numbers		Positive voxel density		AUC35-80		Load (vox number x AUC35-80)	
Group	NL	AD	NL	AD	NL	AD	NL	AD
	Mean(SD)	Mean(SD)	Mean(SD)	Mean(SD)	Mean(SD)	Mean(SD)	Mean(SD)	Mean(SD)
Superior turbinate	**115.1(71.1)***	**39.4(18.5)**	**36.6(22.3)***	**12.5(5.9)**	0.63(0.12)	0.59(0.07)	**71.6(38.3)***	**23.9(13.0)**
middle. turbinate	257.4(227.1)	271.4(176.8)	21.0(18. 6)	22.2(14.4)	0.50(0.10)	0.56(0.07)	121.9(98.8)	153.9(109.8)
orbit	10.0(2.0)	18.6(14.9)	0.95(1.23)	4.51(4.2)	0.26(0.34)	0.44(0.20)	3.0(2.8)	7.9(7.5)
muscle	5.0(5.2)	6.0(5.3)	1.65(2.27)	2.71(2.4)	0.39(0.31)	0.55(0.11)	1.95(2.2)	3.4(3.0)

[0059] To estimate the amount of tracer (CSF) clearance, the regional tracer load was calculated over the 35-80min intervals (Load = positive voxels x AUC). Uniquely, the control superior turbinate region showed greater voxel number ($U=7$, $p=.01$), voxel density ($U=7$, $p=.01$)

and load (U=8, p=.02) than AD. As mentioned above, this interval was selected as both venous and arterial blood TACs were always low and unchanging over this time range. However, for comparison, the 3 min. to 80 min. tracer load was also calculated. Again, it was observed that the superior turbinate load was specifically greater in control as compared with AD (U=8, p<0.02). Closer examination of the data show that the shell AUC measurements do not show group effects (U=24, p>0.05), rather the superior turbinate results are driven by the greater numbers of positive voxels in the controls. Nevertheless, the finding that the NL group had greater tracer load, i.e. greater tracer clearance over the 35-80min. interval than the AD group raised the possibility of greater tracer dilution in the larger AD intracranial CSF pool which was 340.1ml +/- 49.0 as compared with the control 228.4ml +/- 44.3 (U=55, p<0.01). However, statistical adjustment for the CSF volume (Load x CSF volume) did not change the observed increased load result in control (U=9, p<.05). Further, to rule out non-specific tracer binding in nasal structures, it was examined the THK 5117SUVR in the superior and middle turbinates. No binding was observed (mean SUVR=0.59+/- 0.08) and there were no group binding differences U=37, p>0.05) thus likely ruling out a non-specific nasal mucosa tracer uptake as the source for the higher superior turbinate AUC differences as compared with the blood as seen in Figures 5 and 6.

[0060] The hypothesized relationship between the CSF clearance as estimated from both ventricle and superior turbinate sites and the brain deposition of amyloid using 11C-PiB was confirmed. Both the superior turbinate 35-80min. load and ventricular AUC were uniquely associated with amyloid binding to the neocortical gray matter ((rho=-.64, p<0.05) and rho=-.82 p<0.01, respectively see Figure 8). Figure 8 shows scattergrams examining for AD and controls the relationships between amyloid gray matter binding (PiB-PET) and: A). the ventricular CSF AUC; B). the change in the ventricular AUC between 35min and 80min; C). the superior turbinate the load; and D). The change in the superior turbinate load between 35min and 80min. The associations with amyloid binding were not found in any other ROI. The data also show that the change in the counts over 35 min to 80 min was reduced in the ventricular CSF in the AD while the change in the turbinate counts was not significant. It is tempting to interpret the higher AD concentrations as showing that both the superior turbinate and ventricle reflect impaired systemic CSF clearance, but there is a difference in terms of rate at which they are cleared. The ventricle is clearing to other CSF compartments while the turbinates are presumably clearing to the cervical lymphatics and venous blood which do not show disease effects.

DISCUSSION

[0061] While there is excellent evidence across animal species for a CSF egress pathway from the brain through the cribiform plate, minimal evidence exists for the human. Using a post mortem intracisternal dye injection, one study demonstrated a potential nasal turbinate egress pathway in the human, however there are no human in vivo demonstrations. However, that a link does exist in the human is demonstrated that in both animal and human there is an intranasal delivery of macromolecules to the CSF. Example I provides a novel examination of human PET data to offer a view of the CSF-ISF clearance pathway. Our study demonstrates three important results: 1. in all subjects there is evidence for a nasal CSF-ISF drainage pathway; 2. In AD, the tracer concentrations are higher in the ventricular and superior turbinate CSF suggesting clearance is reduced. This finding is anatomically specific to these CSF containing regions; and 3. The CSF concentration measures (surrogates for clearance to the CSF) are associated with the increased deposition of brain Aβ. Importantly, the estimates of clearance from these structures shows a defect only for the ventricle and not for the superior turbinates.

[0062] The method of Example I is designed to evaluate CSF egress out of the brain by examining the time course and concentration of tracer counts following an IV injection of a PET radioligand. The method involves three steps, first for each subject a shell region, outside of the brain and subarachnoid space, containing bone and soft tissue is created. Second, possible CSF sites are identified by identifying in the shell, voxels with a high temporal correlation with the ventricular counts. It was observed that all subjects demonstrated positive superior turbinate voxels. Third, to further characterize the positive voxels as CSF-like anatomical regions of interest were created and the positive voxels within these regions were tested. The tests were designed to compare the positive voxels with respect to "pure" CSF, blood, and brain.

[0063] The results show that region below the cribiform plate, the superior turbinate, had the greatest density of highly correlated voxels whose intensity (concentration), as compared with other shell regions, were consistent with CSF and not to brain or blood. While the study of Example I is unable to demonstrate definitively that the counts measured in the nasal region originated from the brain subarachnoid space, there is additional supportive evidence derived from average counts from other tissues. Between 35 and 80 min, 18F-THK5117 intensity levels are becoming increasingly stable across all tissues. Across this time frame it was observed that the average counts in the nasal region did not differ from those from the ventricular CSF. Rather, the nasal counts

were significantly higher than the arterial and venous blood counts, and as expected, the two blood measures were not different from each other. The counts from the brain were significantly higher than nasal counts.

[0064] Further, all regions were anatomically distant from brain and all results remained significant after partial volume correction. The individual shell ROI's were tested for evidence of tracer binding, and did not find any evidence for this. Blood tracer contamination was limited by restricting our concentration measurements to a period well after blood tracer activity levels had returned to baseline levels. Simulations were performed and concluded the effects of regional CBF are negligible on the AUC. Therefore, it is believed that the nasal turbinate counts were derived from the brain's CSF pool and not contaminated from either brain or blood. Overall, these data are consistent with the hypothesis that there is CSF egress from the brain to the superior nasal turbinates in the human. As such, a dynamic PET scan can provide evidence for the egress of CSF from the human brain through the nasal turbinates.

[0065] Example I demonstrates that using PET of a CSF egress to the nasal turbinates and ventricle that is reduced in AD is of potential clinical interest. The AD related defects detected in CSF clearance at the ventricle and superior turbinate rely on the performance of a small PET based radiotracer where the kinetics of brain penetration, binding and exit remain poorly characterized and may contribute to magnitude estimation errors. In other words, membrane permeability could affect the timing of brain delivery of tracer to ventricle and non-brain regions which formed the basis of our detection of non-brain CSF signals. While these effects do not invalidate detection of CSF shown in Example I, it does potentially impact on the interpretation of the magnitude of CSF removed. The PET tracers while small <5kd still have a greater molecular weight than the CSF/ISF, a difference that could contribute to underestimating the volume of CSF egress. Further, the production of CSF, which was not examined in Example I may also be reduced in the patient sample who are known to have a larger brain CSF pool. These differences of course could directly influence the estimated egress as the net tracer in should equal the amount cleared plus the bound fraction. Here, the brain CSF volumes were directly measured and it was demonstrated that after adjustment the estimated reduced tracer clearance from the CSF remained reduced in AD. However, it did not control for the large fraction of CSF in the spinal column, even though this is not known to be a principal site for absorption or affected by AD. In healthy adults, the CSF is

replaced every 8 hours whereas in AD this has not been estimated and consequently the overall effects remain unknown.

[0066] Example I shows that a reduced tracer efflux at the turbinates and ventricle are associated with an increased brain Aβ binding as determined using 11C-PiB PET. Although the method of Example I does not directly measure tau or Aβ clearance, CSF Aβ clearance may be reduced in AD *in vivo* while the production of Aβ appears unaffected. As such, it is believed that once the Aβ is transported to the ISF (after possible delay at the brain CSF barrier), the rate of clearance afterwards is highly dependent on the CSF bulk flow our method estimates. The data of Example I support a mechanism where reduced solute clearance in AD is related to elevated brain Aβ levels. In summary, prior human Aβ clearance observations directly measure the whole body turnover of Aβ, but do not image the brain. Consequently, the relationship of Aβ clearance pathology to CSF drainage remains unknown. On the other hand, the method of Example I estimates CSF drainage but does not directly measure Aβ clearance.

[0067] The dilution and rate of tracer (CSF) removal from a limited aspect of the potentially relevant anatomy was estimated. Specifically, CSF egress along the spinal column was not characterized due to the limited field of view of the image acquisitions, and egress from the brain subarachnoid space was also not characterized due to spatial resolution limitations inherent with the PET technique. With a camera resolution of approximately 4-6mm the higher count signals from brain confound the lower subarachnoid sampling. Example I manages the distance of the nasal turbinate ROI from brain, and uses partial volume corrected data to provide some measure of control over potential errors. The results of Example I show that the nasal turbinate signal over the last 35 minutes of the study are more closely related to ventricular CSF than to either blood or brain.

[0068] Example I demonstrates a potentially complimentary view to other methods examining the efflux of solutes from brain ISF and CSF. As such this method may be of useful in neurodegenerative and possibly other brain diseases where inflammation or metabolic alterations may affect the bulk CSF flow. This method may have some early advantages as IV PET tracer administration is less invasive than intrathecal MR contrast administration, but has the disadvantages of radiation exposure and long study durations.

[0069] In conclusion, using PET, Example I shows in human evidence for the bulk flow of CSF from the brain to the superior nasal turbinates. Analysis of the tracer counts showed the counts

in the nasal turbinates were most similar to ventricular CSF as compared with either blood or brain. Based on a comparison between Alzheimer patients and controls and it is observed that: 1. the tracer (CSF) clearance is reduced in AD; and 2. the CSF clearance reduction in AD is related to the extent of Aβ deposition in the brain. Overall, these data point to the potential for a novel site for the non-invasive biomarker for human CSF clearance.

Example II

MATERIALS AND METHODS

Participants and clinical procedures

[0070] An ethics committee approved written informed consent was obtained from all participants or their legal care takers. AD patients were recruited from the memory clinic of Tohoku University Hospital. The AD and healthy normal (NL) controls diagnoses were based on standardized neuropsychological and clinical assessments. All participants received a high resolution T1 weighted MRI. AD was diagnosed at a consensus conference according to the National Institute of Neurological and Communicative Disorders and Stroke/AD and Related Disorders Association criteria.

[0071] 15 subjects were studied with dynamic PET using the ^{18}F-THK5117 tracer. This included 7 NL controls (3 females and 4 males age 74.1±5.6, range 67-83 years, MMSE 28.6±1.6, Clinical Dementia Rating (CDR) = 0, and education 14.6±2.2 years) and 8 probable AD (2 females and 6 males, age 79.8±10.6, range 57-89 years, Mini-Mental State Examination (MMSE) 18.5±4.6, CDR 2.0±0.8, and education 12.1±2.7 years).

[0072] Ten of these subjects, 5 NL and 5 AD also received a ^{11}C-PiB PET scan showing that 3/5 NL and 5/5 AD were PiB positive.

Image acquisition and processing

[0073] **Dynamic PET acquisition:** The PET radiotracers were administered in two imaging sessions within 2 weeks. The radiotracer (18)F-labeled arylquinoline derivative 6-[(3-18F-fluoro-2-hydroxy)propoxy]-2-(4-methylaminophenyl)quinoline or ^{18}F-THK5117, was developed and validated for binding to neurofibrillary tangles and neuropil threads. The second radiotracer, Pittsburgh compound B (^{11}C-PiB), an analog of thioflavin T is a validated biomarker for brain beta-amyloid (Aβ) plaques. Both tracers were prepared at the Cyclotron and Radioisotope Center of Tohoku University, both have low molecular weight (<5KD) and both freely cross the blood-

brain barrier. 185 mBq of ^{18}F-THK5117 and 296 mBq of ^{11}C-PiB were administered by IV bolus injection. PET data were acquired axially along the cantho-meatal plane in list mode continuously for 90 min using a SET-3000 G/X PET scanner (Shimadzu, Kyoto, Japan). Fig. 11 lists the timing of the reconstructed PET image frames. The scanner is equipped with high energy resolution germanium oxyorthosilicate (GSO) scintillators that provide 4.5 mm (transverse) and 5.4 mm (axial) spatial resolutions (full width at half maximum, at 10 cm off axis) and sensitivity of 21 cps/kBq. Attenuation correction was based on transmission image from a rotating 137-Cs point source. The field of view for the PET scans superiorly encompassed the skull and inferiorly the foramen magnum and maxilla.

[0074] MRI acquisition: Each subject received a high-resolution MRI on a GE SIGNA 1.5 T magnet (General Electric, Milwaukee, WI, USA). The protocol included a T1-weighted SPGR gradient echo axial sequence with parameters: echo time/repetition time, 2.4/ 22 ms; flip angle 20°; acquisition matrix 256×256x110; 1 excitation; axial field of view 22 cm, bandwidth 122Hz/px, 0.86 x 0.86 x 1.0 voxel size. In all cases, the MRI field of view (FOV) covered the PET FOV. MRI reformatted to the native PET space was used for regional tissue segmentation and PET partial volume correction.

[0075] PET Image Workflow: The images from both PET tracers were reconstructed to a 128 x 128 x 79 matrix of 2 x 2 x 2.6 mm voxels. After decay correction, standardized uptake value (SUV) images were created by normalizing radioactivity by injected dose and body weight. Each dynamic PET frame was coregistered with the corresponding T1 weighted MRI using Statistical Parametric Mapping (SPM 12) software (www.fil.ion.ucl.ac.uk/spm). PET images were sampled in their original space and partial volume corrected using a modified one tissue model.

[0076] MRI Regional Segmentation: To test for the hypothesized nasal turbinate egress portal, using SPM12, an extra-cranial shell region of interest (ROI) was defined on MRI. The shell included scalp, bone and soft tissues (muscle, nasal turbinates, and globes of the eye) and extended inferiorly to the foramen magnum and maxilla. It excluded brain, subarachnoid CSF, and air. The extra-cranial shell region (A-D) is shown at the exterior of the patient's head in light grey. The following subregions were examined: A. the superior and middle turbinates; B. pterygoid muscle; C. globes of the eye and superior turbinate; and D. the ventricular CSF.

[0077] The following shell ROIs were drawn on the MRI blind to the PET data for specificity testing:

1. The superior nasal turbinates were sampled at a distance 5.2mm (2 voxels) inferior to the frontal lobe in order to minimize partial volume effects from brain. The anterior boundary was at the crista galli. The dimensions of the region were 18 mm anterior-posterior (A-P), 14mm left-right (L-R), and 10mm cranio-caudal (C-C).

2. The middle nasal turbinates were sampled inferior to the superior turbinate. The dimensions of this ROI were: 34mm A-P, 16mm L-R and 18mm C-C.

3. The globes of the eyes and lateral pterygoid muscle were sampled bilaterally and both ROIs were 12mm A-P, 12 L-R, and 6mm C-C.

[0078] The MRI brain was segmented into: lateral ventricle, neocortical gray and white matter, and cerebellar hemisphere gray matter using Free-Surfer (V. 5.1, http://surfer.nmr.mgh.harvard.edu). The ventricular CSF ROI was modified by shrinking the outer ependymal margin by 2 voxels (4mm) to minimize partial volume contamination from brain tissue. Image-derived arterial blood tracer concentrations were sampled from the internal carotid artery and venous blood sampled at the junction of the superior sagittal and transverse sinus.

[0079] **Mapping CSF clearance in the shell:** To identify and anatomically map CSF positive signals in the shell for each subject, we applied a "seeding" procedure similar to one used to identify neural networks in resting fMRI analyses. Using SUV data, the time activity curve (TAC) of every shell voxel from 3-80min, was correlated (Pearson Product r) with the 3-80min TAC from the ventricular CSF.

[0080] For each subject, we identified and anatomically mapped CSF positive voxels in the shell region. For every shell voxel (v), a time activity curve (TAC) was correlated (Pearson Product r) with the TAC from the ventricular CSF. The correlations were derived from 14 time points spanning a 3-80 min interval. Formally, if $t_1, t_2, \ldots. t_n$ are time points in a dynamic PET acquisition, $y_i = v(t_i)$ is the time activity curve of a shell voxel and $x_i = CSF(t_i)$ the time activity curve from CSF, and x and y bar indicate the average value:

$$r = \frac{\sum x_i y_i - n\,\bar{x}\bar{y}}{\sqrt{(\sum x_i^2 - n\bar{x}^2)}\sqrt{(\sum y_i^2 - n\bar{y}^2)}}$$

[0081] Fig. 12 illustrates this concept on two sample time activity curves. Shell voxels correlated with ventricular CSF with $r \geq .95$ were considered CSF positive. The figure shows a reference TAC for CSF (top) and TAC for two sample shell voxels: middle = voxel highly

correlated with CSF, r = .98; and the lower curve shows lower correlation r = .88. The correlations were based on the 3-80min time frames.

[0082] Voxels whose correlations were r >.95 were considered potentially CSF positive and further tested for tracer concentrations.

[0083] **Tracer concentration estimations and CSF validation:** Voxel tracer concentrations were derived from the SUV data normalized by the corresponding cerebellar gray matter time frames and examined as area under the curve (AUC). The 35-80min time period ($AUC_{35\text{-}80min}$) was selected because blood concentrations were consistently low. A prior PET kinetic study of ^{18}F-THK5117 also confirmed that arterial plasma concentrations were near baseline levels by 35min. CSF validation of the positive shell voxels was determined by contrasting their tracer concentrations against the concentrations from ventricular CSF, blood, and brain.

[0084] **Measures of tracer binding:** Conventional time frames used to estimate tracer binding were: 50-80min for ^{18}F-THK5117 and 50-70min for ^{11}C-PiB. Both measures were normalized by their respective cerebellar gray matter SUV to form the SUV ratio (SUVR). For both tracers, SUVR values $\geq$ 1.5 defined positive voxels.

Statistical analysis:

[0085] Non-parametric tests were used to test the major hypotheses. Correlations were examined with Spearman tests and partial correlations using Quade's "index of matched correlation". Between group contrasts were made with the Mann-Whitney U. Within subject anatomical specificity tests were examined with the related samples Wilcoxon Signed Rank Tests. The Holm-Bonferroni method for multiple comparisons was used for p value adjustment. All tests were two-sided and statistical significance was set at $p<.05$ when not adjusted for multiple comparisons.

RESULTS

Study 1. Anatomical distribution and validation of nasal cavity CSF.

[0086] **Global distribution:** The TAC correlation analysis across all subjects consistently showed a three-fold greater percentage of ventricle correlated extracranial voxels in the nasal cavity than in the rest of the total shell. Fig. 13 shows for 15 subjects, the percentage distribution (+/- SEM) of shell and nasal cavity voxels whose tau PET derived TAC are correlated with the ventricular CSF TAC, within the range of r= .90-.99. The data show a 3 fold greater percentage of

CSF correlated voxels in the nasal cavity than in the total shell. Shell voxels correlated at r>.95 were considered CSF positive.

[0087] **Regional distribution of extracranial CSF:** Consistent with a hypothesized turbinate CSF egress site, 100% of subjects had CSF positive voxels in the superior turbinate ROI. Over all subjects, the highest density of CSF positive voxels was in the superior and middle turbinate ROIs. Both superior and middle turbinates show >23% CSF positive voxels in their ROIs while the ROIs for the globe of the eye, pterygoid muscle, and total shell showed low densities (<5%) of CSF positive voxels (see Table 3). Table 3 shows CSF positive voxel characteristics in regions of the shell, n=15.

Table 3.

	Superior turbinates	Middle turbinates	Eye	Muscle	Shell
Number Voxels in ROI	315	1160	360	216	181621 (23086)
Number Positive Voxels	74.7 (61.7)	264.9 (194.4)	15.4 (13.2)	5.62 (5.08)	7139.0 (3520.8)
ROI Positive Voxel density%	23.7 (20.1)	22.8 (15.9)	4.3 (3.6)*	2.6 (2.3)*	3.9 (2.0)*
Tracer Concentration (mean SUV 35-80 min)	1.27 (.25)	1.12 (.23)*	0.71 (.58)*	0.86 (.51)*	1.09 (.11)*

Values are mean (sd)

* = different from superior turbinate, Wilcoxon Signed Rank Test p<.02

[0088] These results were unchanged after partial volume correction (Table 4). Table 4 shows partial volume corrections for tracer concentrations in Table 3.

Table 4

SUV(35-80)	S. turbinate	M. turbinate	Eye	Muscle	Shell
	1.26(.24)	1.12(.23) *	.71(.58) *	.83(.50) *	1.06(.11) *

Data show Mean SUV 35-80min (SD)

* = different from superior turbinate, Wilcoxon Signed Rank Test p<.01

[0089] A high density of nasal turbinate CSF signals was independently confirmed in 4 normal subjects using 11C-cocaine, a PET tracer with relatively rapid brain clearance, and without nasal turbinate binding.

[0090] Dynamic PET studies of 40 min duration were carried out with a CTI 931 tomograph after injection of 6–8 mCi of [11C]-cocaine. It is believed that there is rapid clearance and weak cortical binding of the tracer. It was observed there was no nasal turbinate binding of the tracer in the 4 subjects studied.

[0091] The correlation between the ventricle sample ("peeled" 2 voxels around the ventricular margins) and all shell voxels was conducted as described in the text. To avoid partial volume errors, this procedure requires a relatively large ventricle to obtain a CSF sample. Consequently, the study was limited to older subjects who typically have larger ventricles. As observed with the THK5117 tau tracer, the highest density of presumed CSF positive sites is in the superior and middle turbinate regions.

[0092] **Concentration based validation of the positive shell voxels.** The CSF origin of the correlated superior turbinate voxels was supported by tracer concentration analyses of the SUV data (see Figure 14). Fig. 14 shows the averaged tau tracer counts (SUV) +/- SEM for all study subjects plotted over 35-80min. Tracer concentrations from CSF positive superior turbinate and ventricular CSF do not differ from each other, but both are significantly different than blood and brain (p's<.05). The average tracer concentration over 35 to 80min from the CSF positive superior turbinate voxels (1.27+/- 0.25), did not differ from the ventricular CSF (1.27 +/- 0.34, p>.05. However, CSF positive superior turbinate voxels had significantly lower tracer concentrations than brain (2.69 +/-0.40, W=3.41, p<0.01) and were higher than blood (arterial 0.94 +/- 0.31, W=-2.56, $p \leq .01$, and venous 0.96 +/- 0.22, W=-2.33, p<.05).

Study 2. CSF clearance in AD

[0093] Figures 15-17 show ventricle and superior turbinate CSF clearance in AD. As compared with NL, AD subjects show: reduced magnitude of ventricular tracer (AUC35-80min)(see Fig. 15), reduced rate of ventricular tracer clearance (see Fig. 16), and a lower number of CSF positive superior turbinate voxels (see Fig. 17).

[0094] The ventricle $AUC_{35\text{-}80min}$ was significantly lower in AD as compared with NL (.53 +/- .08 and 69 +/- .09 respectively, U=7, p=.01) as was the rate of ventricular CSF clearance (.29 +/- .08 and .43 +/- .10 respectively, U=4, p<.01, see Fig. 15 and 16). Fewer CSF positive superior turbinate voxels (clearance sites) were found in AD (39.4 +/- 18.5 vs 115.1 +/- 71.1, U=7, p=.01, see Fig. 17). These results were unchanged after partial volume correction. Both the ventricular

$AUC_{35\text{-}80min}$ and the CSF rate of change showed 80% binary diagnostic agreement with the number of superior turbinate sites (both Kappa's=0.60, p<.05).

Study 3. CSF clearance and amyloid positivity.

[0095] 8 subjects, 5 AD and 3 NL were ^{11}C-PiB PET scan positive. Figures 18 and 19 show the relationship, for 8 PiB positive subjects, between the amyloid binding SUVR. Figure 18 shows the ventricular tracer $AUC_{35\text{-}80min}$ and Figure 19 shows the rate of ventricular tracer clearance. As shown in Figs 18 and 19, both the ventricle $AUC_{35\text{-}80min}$ and the rate of ventricular CSF clearance were inversely correlated with the magnitude of amyloid binding (rho=.93, p<.01 and rho=.74, p<.05, respectively). The superior turbinate data did not reach significance in the correlation with the amyloid binding.

[0096] **Examination of Confounds.** Five potential confounds were examined for their possible effect on the results. First, elevated tau binding in AD would be expected to reduce the available tau tracer to be cleared to CSF, thus lowering the ventricular $AUC_{35\text{-}80min}$. The extent of this effect was estimated by comparing the ventricular $AUC_{35\text{-}80min}$ after cerebellar normalization, a reference region without specific binding, with whole brain normalization, which includes all tau binding sites (see Figures 20 and 21). Figs. 20 and 21 show that compared with NL, AD subjects show lower ventricular $AUC_{35\text{-}80min}$ with both cerebellar gray matter normalization (p=.01)(see Fig. 20) and total brain parenchyma normalization (p<.01)(see Fig. 21). These data suggest large between group clearance differences with relatively smaller contributions from overall tracer retention.

[0097] Relative to cerebellar normalization, whole brain normalization reduced the AUC by 28% in normal and 31% in AD, but the between group AUC difference remained significant (U=5, p<.01). This suggests a relatively greater between group tracer clearance effect than tracer binding effect. Similarly, after statistical adjustment for the total brain binding, the between group ventricle $AUC_{35\text{-}80min}$ effect remained significant (F=7.8, p=0.02). Second, partial volume errors for the ventricular and extracranial regions were minimized by individually sampling the PET at a 4mm distance or greater from brain. Additional partial volume corrections did not change the region or group contrasts. Third, the effect of the larger AD ventricle (58.3mL +/- 14.1) was examined as compared to normal (32.2mL +/- 11.9, U=50, p<0.01) on the ventricle tracer measurements. After statistical adjustment for ventricular volume, the ventricle $AUC_{35\text{-}80min}$ remained lower in AD (F=5.0 p<0.05) and the ventricular rate of signal change was (F=5.0 p<.05). Fourth, no ^{18}F-

THK5117 binding was observed in the nasal turbinates and there were no between group turbinate binding differences (SUVR-Normal=0.56+/- 0.10 and SUVR-AD 62+/- 0.06). These data rule out contamination from the nasal mucosa. Fifth, the effects of reduced flow on the $AUC_{10\text{-}35min}$ and $AUC_{35\text{-}80min}$ was modeled across a wide range of blood flows. The results demonstrate negligible flow effects after 10min thus supporting a conservative 35min start point.

DISCUSSION

[0098] All mammals show evidence of bulk flow CSF egress with some species differences. In common are pathways involving: choroid plexus, cerebral ventricles, perivascular spaces, peri-neural pathways, and lymphatic and capillary exchange to venous blood. In all mammals examined, including those with and without arachnoid granulations (the rodent), a cribriform plate CSF egress pathway is found. However, in the human, owing to limited in vivo accessibility, CSF clearance pathways are less well understood. A principal human egress portal is believed to be via arachnoid granulations located in brain and spinal cord, but its significance is disputed. Our results suggest that CSF clearance can be detected in the human lateral ventricle and nasal turbinates. It was observed that: 1. All subjects demonstrate ventricular CSF clearance and superior turbinate CSF clearance sites, suggesting normal CSF pathways; 2. Compared with control, AD subjects show reduced ventricular tracer clearance as estimated by AUC and slope measures and fewer turbinate sites clearing CSF; and 3. For subjects with positive amyloid binding, the magnitude of binding is inversely associated with ventricular CSF clearance.

[0099] For all subjects, the superior turbinates have two unique properties: the highest regional density of CSF correlated voxels whose tracer concentration is consistent with the ventricular CSF, but different from brain, muscle, and blood. Other extracranial sites including the middle turbinates, globe of the eye, and pterygoid muscle did not share these characteristics. These results are anatomically consistent with in vivo rodent and post mortem cisterna magna dye injections in large mammals including humans that identified a CSF egress pathway traversing the cribriform plate to the superior turbinates and to nasal cavity lymphatics. Other human evidence for a nasal CSF pathway comes from demonstrations of rapid intranasal delivery of macromolecules to the CSF.

[00100] It was observed that in AD there was reduced turbinate egress portals and the reduced concentration and rate ventricle tracer clearance are consistent with reports in rodent AD models of reduced glymphatic (CSF) clearance. The correlated timing of tracer delivery from ventricle to

extracranial sites, the basis of our nasal turbinate CSF detection strategy, could be limited by obstacles to CSF flow. Perivascular CSF channels show well described Aβ accumulations in AD brain, suggesting potential egress site estimation errors. Additionally, the estimates of nasal tracer concentrations are not precise owing to the relatively poor spatial resolution and resultant partial volume errors. Spatial resolution limitations may have accounted for the turbinates to show tracer concentrations consistent with ventricular CSF across all subjects, but owing to decreased numbers of AD related turbinate egress portals and small sample size, to show only trend reductions in AD. Spatial resolution limitations also limited measurement of CSF clearance from the subarachnoid space. On the other hand, the larger lateral ventricle provides good CSF tracer concentration estimates and was a better CSF clearance biomarker. The ventricular measures showed both high diagnostic accuracy and excellent correlation with amyloid binding.

[00101] It was observed that there is a reduced CSF clearance in AD and an inverse association between elevated brain Aβ levels and lower ventricular CSF clearance. Mechanistically, it was observed that reduced solute clearance increases the residence time for Aβ, thus promoting protein misfolding, aggregation, and increased brain Aβ plaques. Further, it is believed that different size molecules in the CSF bulk flow have similar clearance rates and it is suggested that reduced CSF clearance is a possible explanation for the observed impaired clearance of labelled Aβ, a large molecule measured after lumbar puncture. Nevertheless, the contributions of membrane permeability pathology, reduced neuronal metabolism, and cardiovascular factors to reduced solute clearance from the CSF remain untested. Consequently, it will be of interest to directly examine human CSF clearance and the clearance of soluble Aβ and other waste products longitudinally and under physiological challenge conditions.

[00102] It was observed that the ventricular tracer $AUC_{35\text{-}80}$, a product of both input from brain and CSF output, was reduced in AD. This finding appears consistent with the increased brain tracer binding found in AD, resulting in less tracer available for clearance. A decreased rate of CSF egress in AD, a finding consistent with a larger AD CSF pool, was also observed. However, controlling for increased binding and ventricular size did not fully explain the AD CSF clearance deficits, thus suggesting a primary damage to the clearance pathway. Overall, where rodent AD models of CSF clearance identify membrane defects (impaired solute movement from tissue to CSF) and impaired solute egress from the CSF to extracranial lymphatics, estimates of impaired tracer trafficking across brain tissue membranes were not made, and therefore the relative

contributions of these two effects was not modeled in Example II. A validation study did rule out reduced cerebral blood flow as the basis for the reduced CSF clearance over the interval studied (>35 min). Clearly, more comprehensive PET models considering the CSF are needed where current quantitative PET models are designed to estimate tracer incorporation into tissue.

[00103] PET has advantages as intravenous radiotracer administration is minimally invasive while offering a conventional diagnostic uptake measure. The PET approach is complimentary to the more invasive methods used in animal experiments in aging, sleep pathology, and neurodegeneration models examining the efflux of solutes to and from brain to CSF and blood. The disadvantages include radiation exposure, the less direct delivery from blood, and longer study durations. Overall, despite obvious spatial resolution limitations and suboptimal tracers, we provide first evidence that dynamic PET yields important insight into CSF flow. Our results highlight the importance of a ventricle clearance biomarker and of exploiting the nasal pathway for the sampling CSF molecules cleared from the brain.

[00104] Dynamic PET was used to estimate systemic CSF clearance in ventricular and extracranial regions. As previously found in other mammals, the results show the human nasal turbinates, are anatomically part of the CSF egress system. In comparisons between AD and NL, we find that ventricular CSF and superior nasal turbinate clearance measures are reduced in AD. Consistent with a proposed proteinopathy mechanism, ventricular CSF clearance was inversely related to Aβ deposition. Consequently, PET based CSF clearance measures may be of interest in the evaluation of the propagation and mitigation of Aβ and other neurodegeneration lesions

[00105] The invention described and claimed herein is not to be limited in scope by the specific embodiments herein disclosed since these embodiments are intended as illustrations of several aspects of this invention. Any equivalent embodiments are intended to be within the scope of this invention. Indeed, various modifications of the invention in addition to those shown and described herein will become apparent to those skilled in the art from the foregoing description. Such modifications are also intended to fall within the scope of the appended claims. All publications cited herein are incorporated by reference in their entirety.

CLAIMS

What is claimed is:

1. A method for *in vivo* detection of cerebrospinal fluid (CSF) egress in a patient, comprising:

intravenously administering a tracer capable of being taken up by brain tissue of the patient and subsequently clearing the brain tissue of the patient;

continuously detecting the tracer in the patient's head and nasal region, and at least a portion of the patient's brain for a predetermined amount of time to obtain tracer data;

correlating the tracer data to a three-dimensional anatomical image of the patient's head, nasal region, and brain; and

estimating a rate or a volume of CSF egress from a brain through a spinal fluid clearance pathway of the patient based the tracer data.

2. The method of claim 1, wherein the tracer binds to the brain.

3. The method of claim 2, wherein the spinal fluid clearance pathway comprises at least one of a cerebral ventricular system, a subarachnoid CSF compartment, and a nasal turbinate.

4. The method of claim 1, wherein the tracer does not bind to the brain.

5. The method of claim 4, wherein the estimating step comprises estimating a rate or a volume of tracer egress from the brain.

6. The method of claim 1, further comprising:

diagnosing a patient with a neurological, inflammatory or cardiovascular disorder based on the rate of CSF egress through the spinal fluid clearance system of the patient.

7. The method of claim 6, wherein the disorder is a disease having abnormal amounts of protein deposits in the brain.

8. The method of claim 7, wherein the disorder is selected from the group consisting of Parkinson's disease, progressive supranuclear palsy, and Alzheimer's disease.

9. The method of claim 6, wherein the disorder is selected from the group consisting of traumatic brain injury, sleep disturbances, stroke and vascular disease, and brain conditions that cause an inflammatory response.

10. The method of claim 1, wherein the tracer is capable of binding to at least one of neurofibrillary tangles, neuropil threads, and beta-amyloid plaques in the brain tissue.

11. The method of claim 1, wherein the tracer is a Positron Emission Tomography (PET) radiotracer.

12. The method of claim 11, wherein the tracer data is obtained using dynamic PET imaging.

13. The method of claim 11, wherein the PET radiotracer is a tau or amyloid protein tracer.

14. The method of claim 13, wherein the PET radiotracer is selected from a group consisting of ^{18}F-THK5517, ^{11}C-PiB, and ^{18}F-THK5351.

15. The method of claim 11 wherein the PET radio tracer is ^{11}C-Butanol or ^{11}C-Cocaine.

16. The method of claim 1, wherein the tracer is a magnetic resonance imaging (MRI) contrast agent.

17. The method of claim 1, wherein the tracer data comprises at least one of time activity curves (TAC), areas under the curves (AUC), and standardized uptake value (SUV) images of the tracer over at least a portion of the predetermined amount of time.

18. The method of claim 1, wherein the three-dimensional anatomical image is a three-dimensional magnetic resonance imaging (MRI) image of the patient's head and nasal region.

19. The method of claim 1, wherein the patient is a human.

20. A method for *in vivo* detection of cerebrospinal fluid (CSF) egress in a patient, comprising:

intravenously administering a tracer capable of being taken up by brain tissue of the patient and subsequently clearing the brain tissue of the patient;

continuously detecting the tracer in the patient's head and nasal region for a predetermined amount of time to obtain tracer data;

identifying one or more voxels within a shell region of interest (ROI) of the patient, wherein the shell ROI is outside the brain and the subarachnoid space, and includes bone and soft tissue; and

estimating a rate of CSF egress through at least one of the voxels within the shell ROI based on the tracer data.

21. The method of claim 20, wherein the shell ROI comprises at least one of dura, muscle, nasal turbinate and orbits.

22. The method of claim 20, wherein a first portion of the tracer data for the one or more voxels are temporally correlated to a second portion of the tracer data for lateral ventricles of the patient.

23. The method of claim 20, wherein a first portion of the tracer data for the one or more voxels is above a predetermined threshold value compared to the tracer data.

24. The method of claim 20, wherein a first portion of the tracer data for the one or more voxels is correlated to an amount of tracer present in the patient's blood.

25. The method of claim 20, further comprising:

diagnosing a patient with a neurological, inflammatory or cardiovascular disorder based on the rate of CSF egress through the spinal fluid clearance system of the patient.

26. The method of claim 20, wherein the disorder is selected from the group consisting of Alzheimer's disease, traumatic brain injury, sleep disturbances, stroke and vascular disease, and brain conditions that cause an inflammatory response.

27. The method of claim 20, wherein the tracer is capable of binding to at least one of neurofibrillary tangles, neuropil threads, and beta-amyloid plaques in the brain tissue.

28. The method of claim 20, wherein the tracer is a Positron Emission Tomography (PET) radiotracer.

29. The method of claim 28, wherein the tracer data is obtained using dynamic PET imaging.

30. The method of claim 28, wherein the PET radiotracer is selected from a group consisting of ^{18}F-THK5517, ^{11}C-PiB, ^{11}C-Cocaine, and ^{18}F-THK5351.

31. The method of claim 20, wherein the tracer is a magnetic resonance imaging (MRI) contrast agent.

32. The method of claim 20, wherein the tracer data comprises at least one of time activity curves (TAC), areas under the curves (AUC), and standardized uptake value (SUV) images of the tracer over at least a portion of the predetermined amount of time.

33. The method of claim 20, wherein the tracer data for each of the voxels are normalized by corresponding data for a cerebellar hemisphere gray matter of the patient.

34. The method of claim 20, wherein the patient is a human.

35. A system, comprising:

an imaging device continuously gathering tracer data corresponding to uptake and clearance, within a brain of a patient, of a tracer intravenously administered to the patient; and

a computing device comprising one or more processors and a set of instructions executing on the one or more processors, the set of instructions being operable to: receive the tracer data from the imaging device, correlate the tracer data to a three-dimensional anatomical image of the patient's head and nasal region, and estimating a rate or a volume of CSF egress from a brain through a spinal fluid clearance pathway of the patient based the tracer data.

36. A system, comprising:

an imaging device continuously gathering tracer data corresponding to uptake and clearance, within a brain of a patient, of a tracer intravenously administered to the patient; and

a computing device comprising one or more processors and a set of instructions executing on the one or more processors, the set of instructions being operable to: receive the tracer data from the imaging device, identify one or more voxels within a shell region of interest (ROI) of the patient, wherein the shell ROI is outside the brain and the subarachnoid space, and includes bone and soft tissue, and estimating a rate of CSF egress through at least one of the voxels within the shell ROI based on the tracer data.

37. A system, comprising:

an imaging device continuously gathering tracer data corresponding to uptake and clearance, within a brain of a patient, of a tracer intravenously administered to the patient; and

a computing device comprising one or more processors and a set of instructions executing on the one or more processors, the set of instructions being operable to: receive the tracer data from the imaging device, correlate the tracer data to a three-dimensional anatomical image of the patient's head, nasal region and brain, and estimating a rate or a volume of CSF egress from a brain through a spinal fluid clearance pathway of the patient based the tracer data.

100

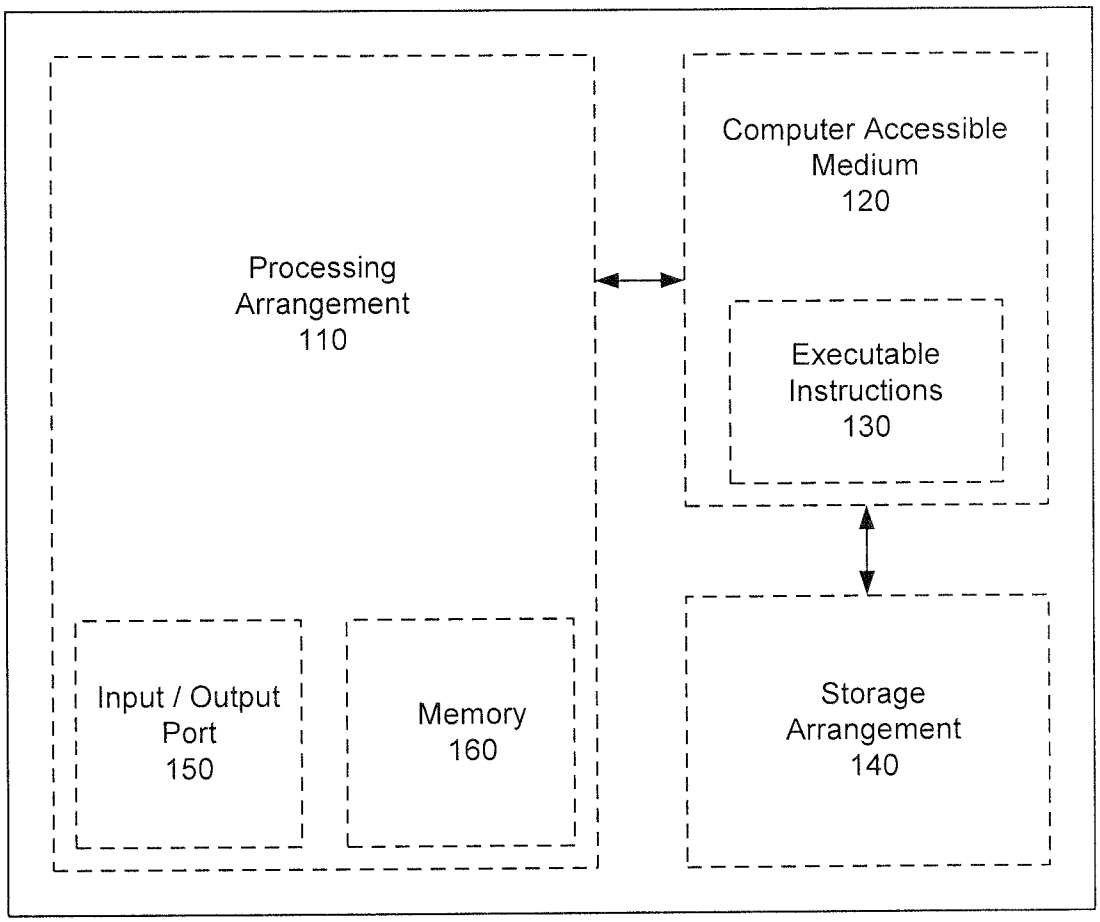
Processing Arrangement 110
Computer Accessible Medium 120
Executable Instructions 130
Input / Output Port 150
Memory 160
Storage Arrangement 140

Fig. 1

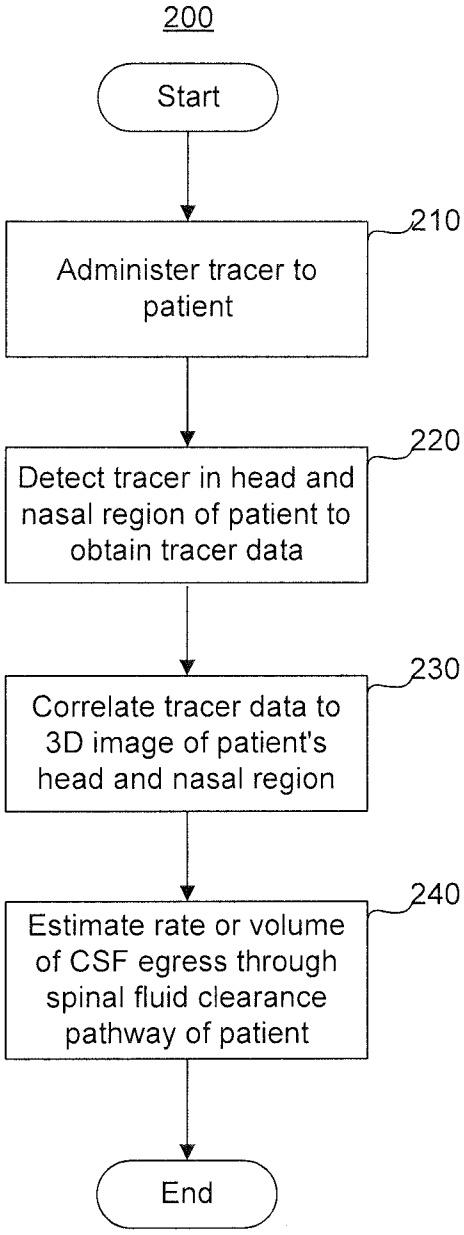
200
Start
Administer tracer to patient
210
Detect tracer in head and nasal region of patient to obtain tracer data
220
Correlate tracer data to 3D image of patient's head and nasal region
230
Estimate rate or volume of CSF egress through spinal fluid clearance pathway of patient
240
End

Fig. 2

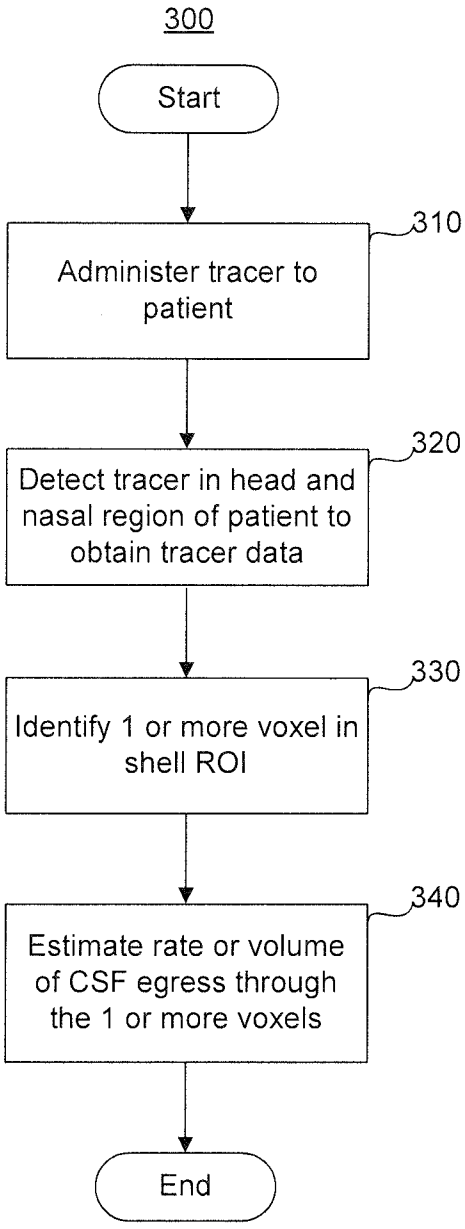
300
Start
310
Administer tracer to patient
320
Detect tracer in head and nasal region of patient to obtain tracer data
330
Identify 1 or more voxel in shell ROI
340
Estimate rate or volume of CSF egress through the 1 or more voxels
End

Fig. 3

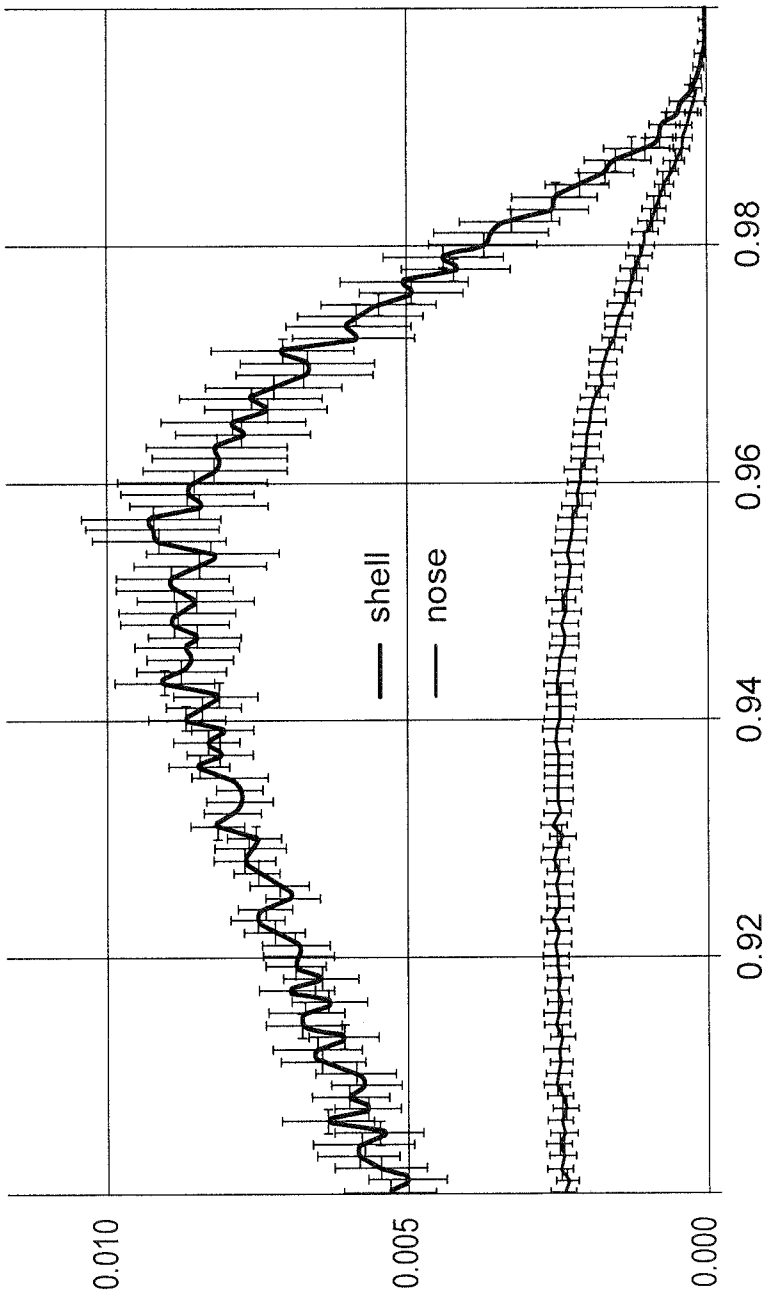

Fig. 4

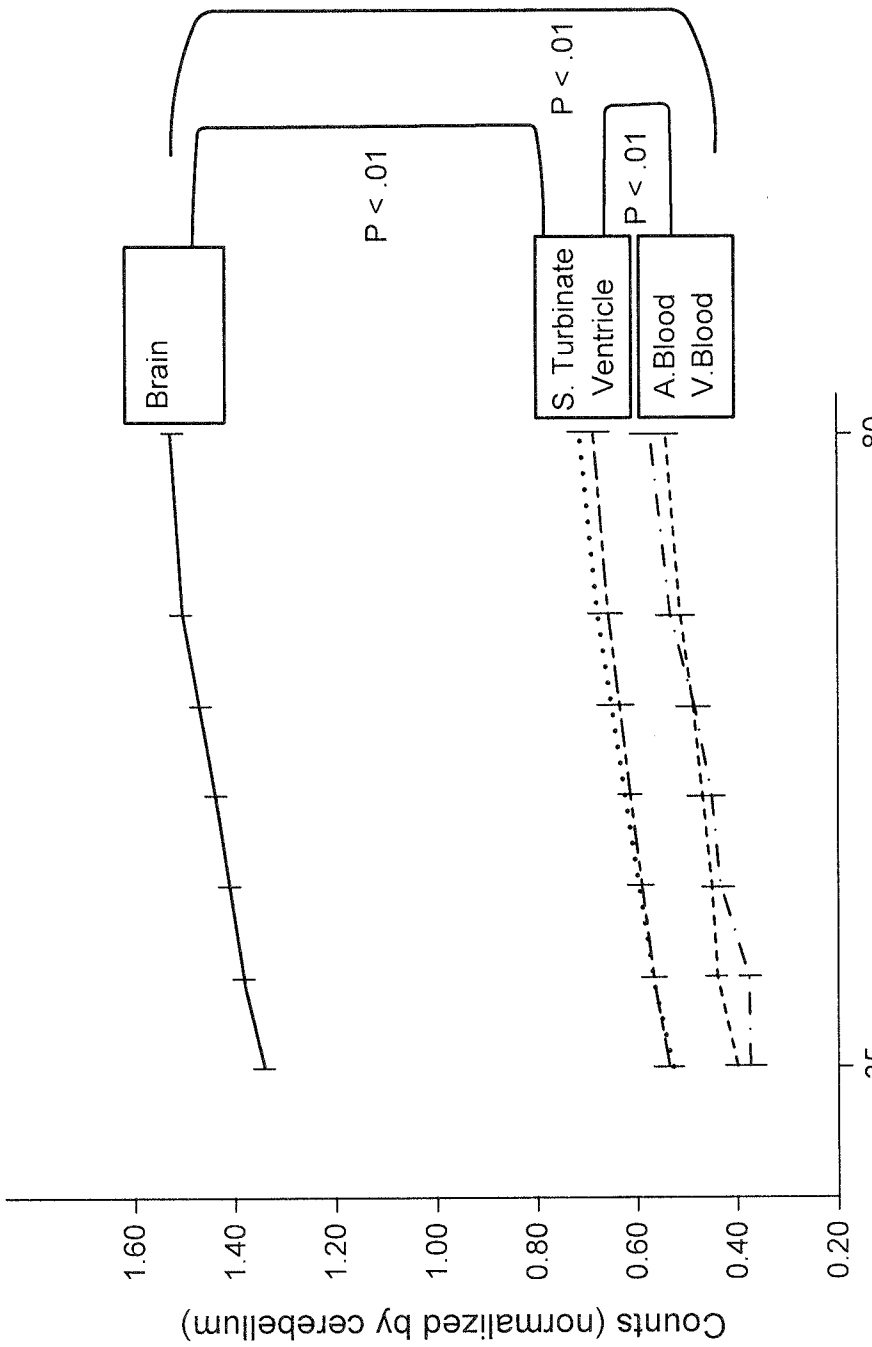
Counts (normalized by cerebellum)
1.60
1.40
1.20
1.00
0.80
0.60
0.40
0.20
35
80
Time
Error Bars: +/- 1 SE
Brain
S. Turbinate
Ventricle
A.Blood
V.Blood
P < .01
P < .01
P < .01

Fig. 5

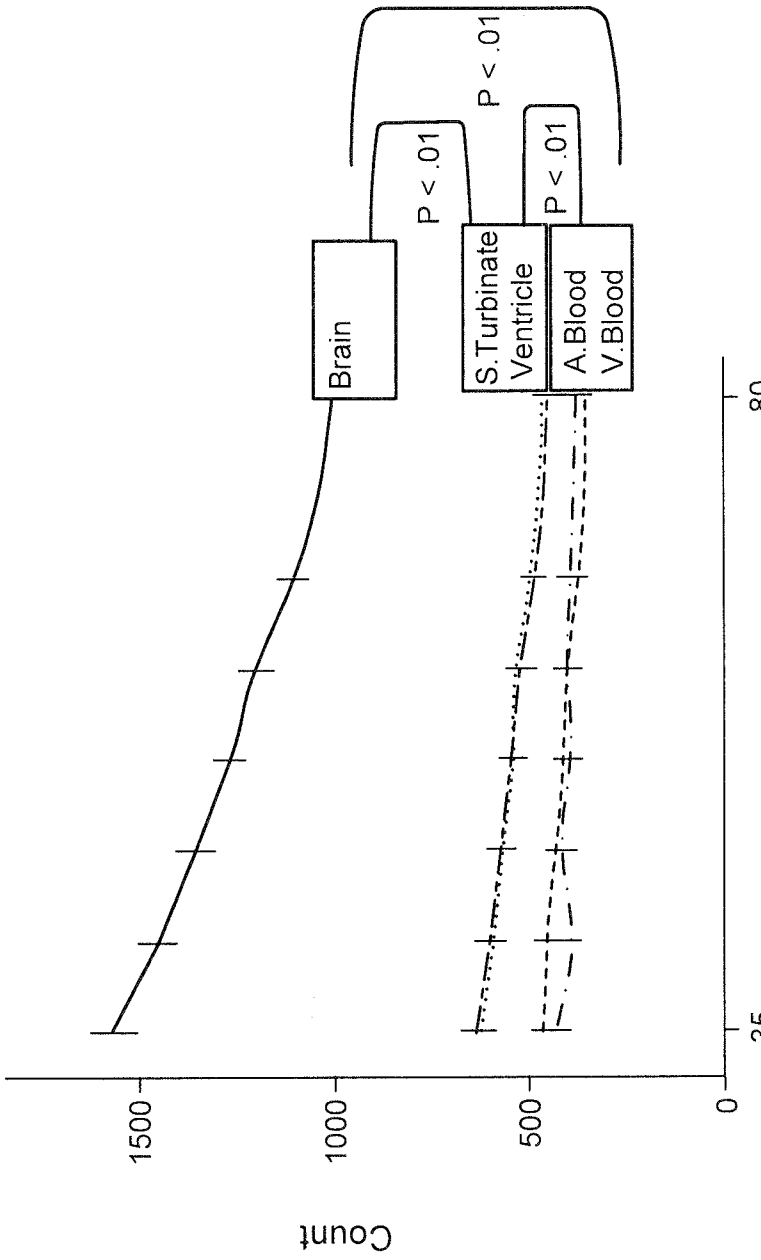
Count
1500
1000
500
0
35
80
Time
Error Bars: +/- 1 SE
Brain
S.Turbinate
Ventricle
A.Blood
V.Blood
P < .01
P < .01
P < .01

Fig. 6

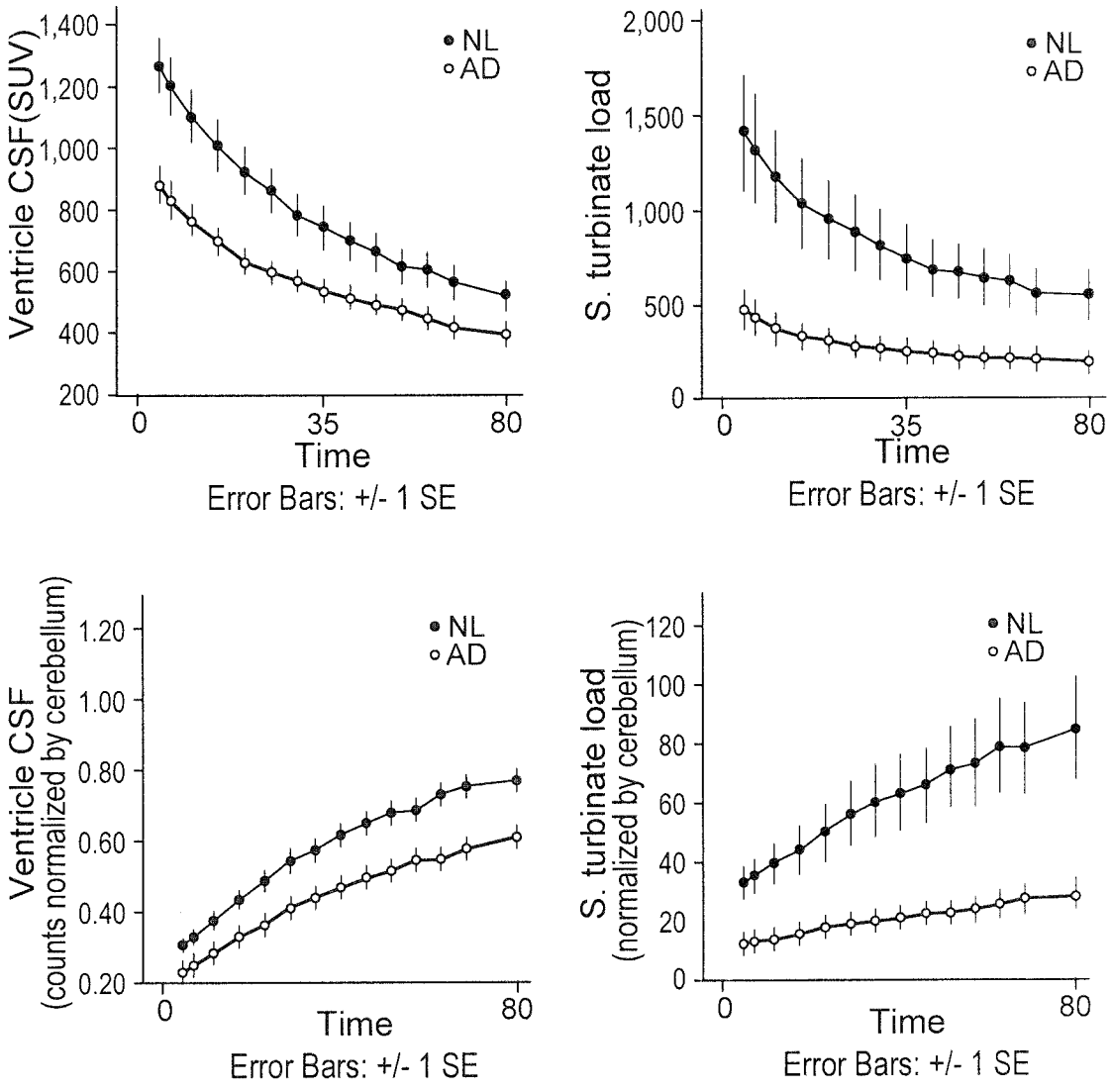
Ventricle CSF(SUV)
1,400
1,200
1,000
800
600
400
200
0
35
80
Time
NL
AD
Error Bars: +/- 1 SE
S. turbinate load
2,000
1,500
1,000
500
0
Ventricle CSF (counts normalized by cerebellum)
1.20
1.00
0.80
0.60
0.40
0.20
S. turbinate load (normalized by cerebellum)
120
100
80
60
40
20

Fig. 7

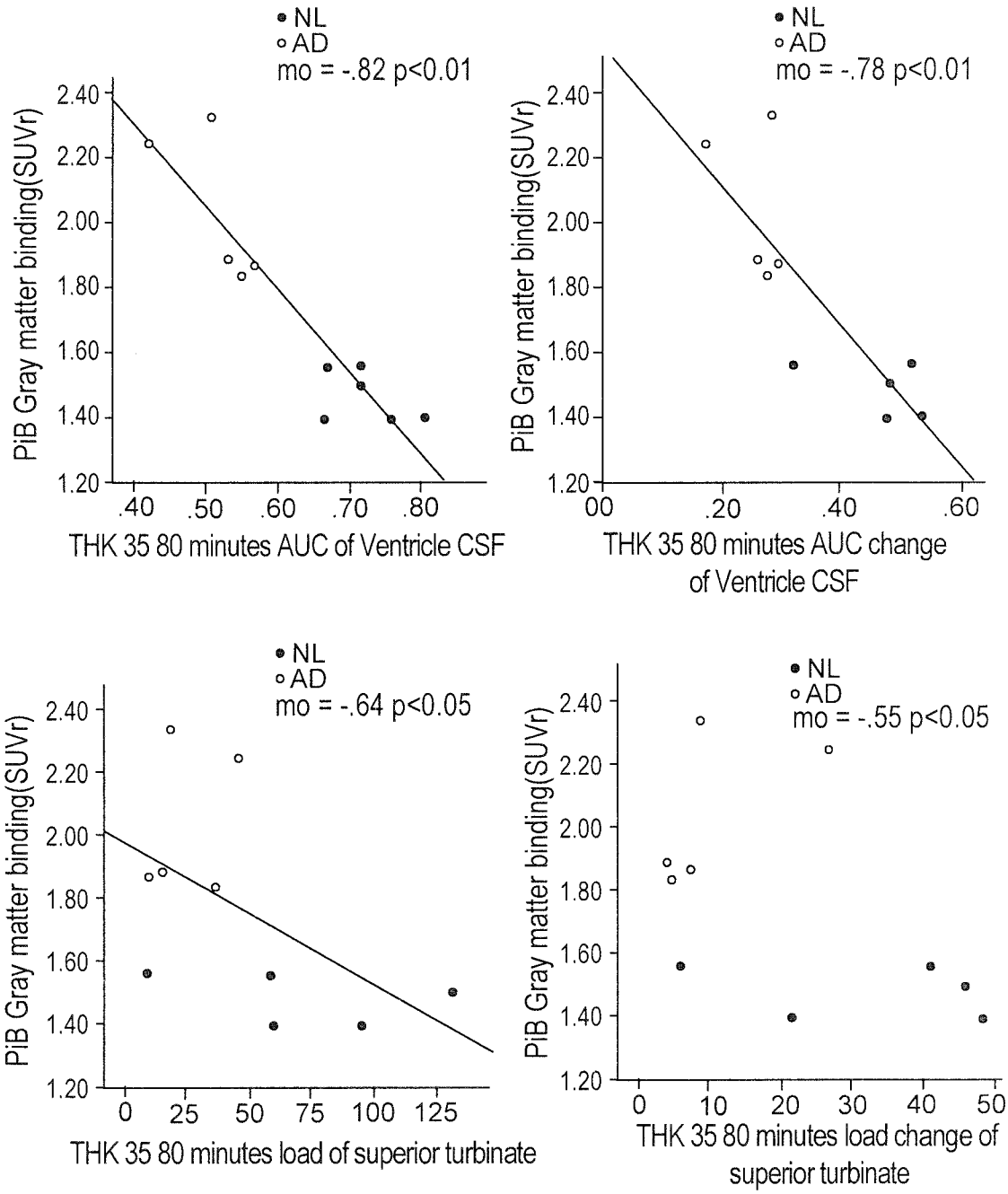
NL
AD
mo = -.82 p<0.01
PiB Gray matter binding(SUVr)
2.40
2.20
2.00
1.80
1.60
1.40
1.20
.40
.50
.60
.70
.80
THK 35 80 minutes AUC of Ventricle CSF
NL
AD
mo = -.78 p<0.01
PiB Gray matter binding(SUVr)
2.40
2.20
2.00
1.80
1.60
1.40
1.20
00
.20
.40
.60
THK 35 80 minutes AUC change of Ventricle CSF
NL
AD
mo = -.64 p<0.05
PiB Gray matter binding(SUVr)
2.40
2.20
2.00
1.80
1.60
1.40
1.20
0
25
50
75
100
125
THK 35 80 minutes load of superior turbinate
NL
AD
mo = -.55 p<0.05
PiB Gray matter binding(SUVr)
2.40
2.20
2.00
1.80
1.60
1.40
1.20
0
10
20
30
40
50
THK 35 80 minutes load change of superior turbinate

Fig. 8

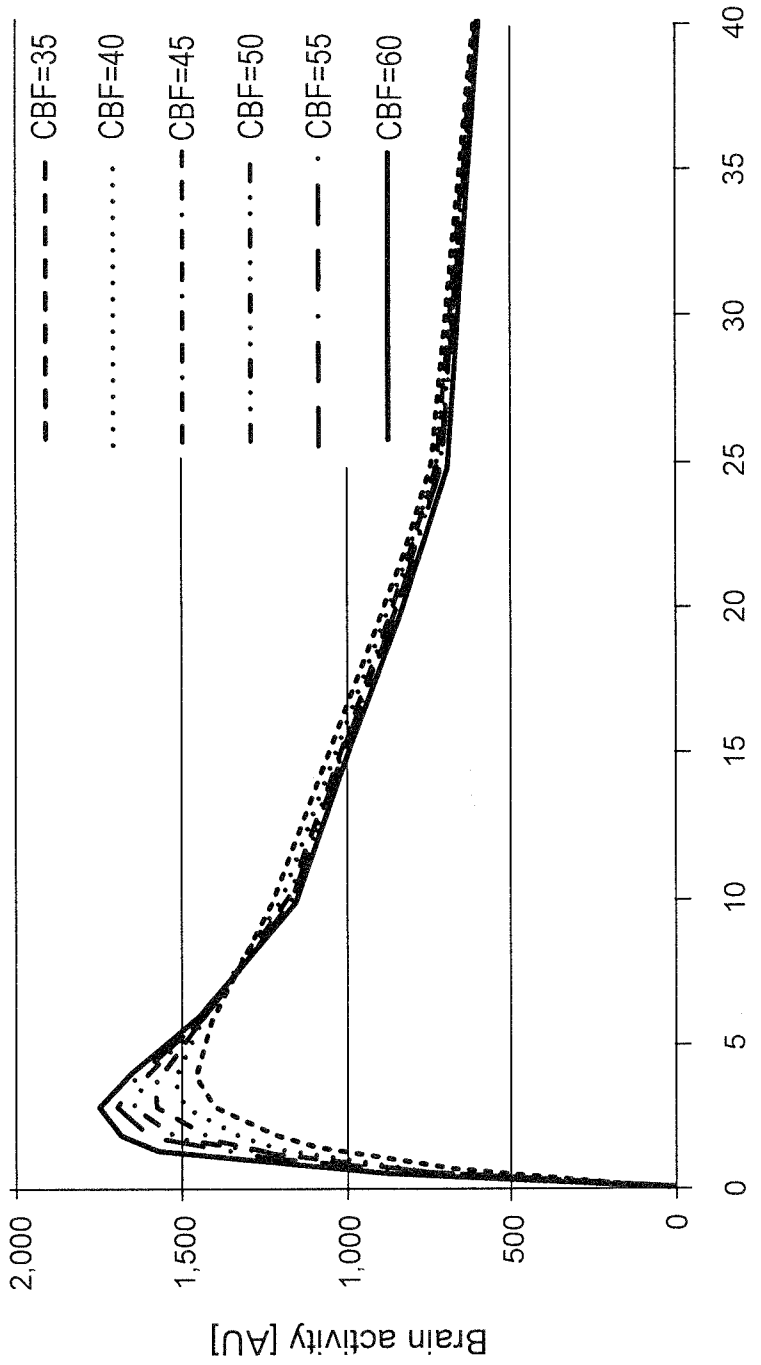
CBF=35
CBF=40
CBF=45
CBF=50
CBF=55
CBF=60
Brain activity [AU]
2,000
1,500
1,000
500
0
0
5
10
15
20
25
30
35
40
Time [mins]

Fig. 9

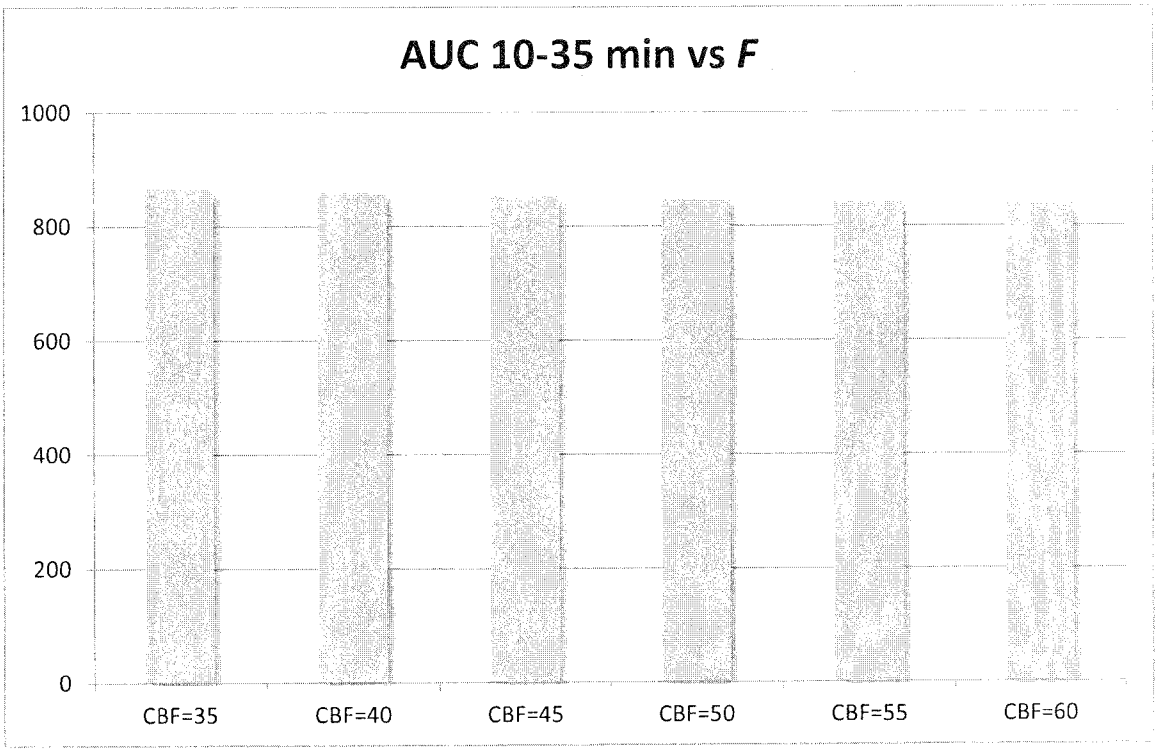
AUC 10-35 min vs F
1000
800
600
400
200
0
CBF=35
CBF=40
CBF=45
CBF=50
CBF=55
CBF=60

Fig. 10

	THK-5117			PiB			
Frame number	duration(sec)	start time(min)	end time(min)	Frame number	scan duration(sec)	start time(min)	end(time)
1	10	0	0.2	1	10	0.0	0.2
2	10	0.2	0.3	2	10	0.2	0.3
3	10	0.3	0.5	3	10	0.3	0.5
4	10	0.5	0.7	4	10	0.5	0.7
5	10	0.7	0.8	5	10	0.7	0.8
6	10	0.8	1	6	10	0.8	1.0
7	10	1	1.2	7	20	1.0	1.3
8	10	1.2	1.3	8	20	1.3	1.7
9	10	1.3	1.5	9	20	1.7	2.0
10	10	1.5	1.7	10	60	2.0	3.0
11	10	1.7	1.8	11	60	3.0	4.0
12	10	1.8	2	12	180	4.0	7.0
13	60	2	3	13	180	7.0	10.0
14	60	3	4	14	300	10.0	15.0
15	120	4	6	15	300	15.0	20.0
16	240	6	10	16	300	20.0	25.0
17	300	10	15	17	300	25.0	30.0
18	300	15	20	18	300	30.0	35.0
19	300	20	25	19	300	35.0	40.0
20	300	25	30	20	300	40.0	45.0
21	300	30	35	21	300	45.0	50.0
22	300	35	40	22	300	50.0	55.0
23	300	40	45	23	300	55.0	60.0
24	300	45	50	24	300	60.0	65.0
25	300	50	55	25	300	65.0	70.0
26	300	55	60				
27	600	60	70				
28	600	70	80				

Fig. 11

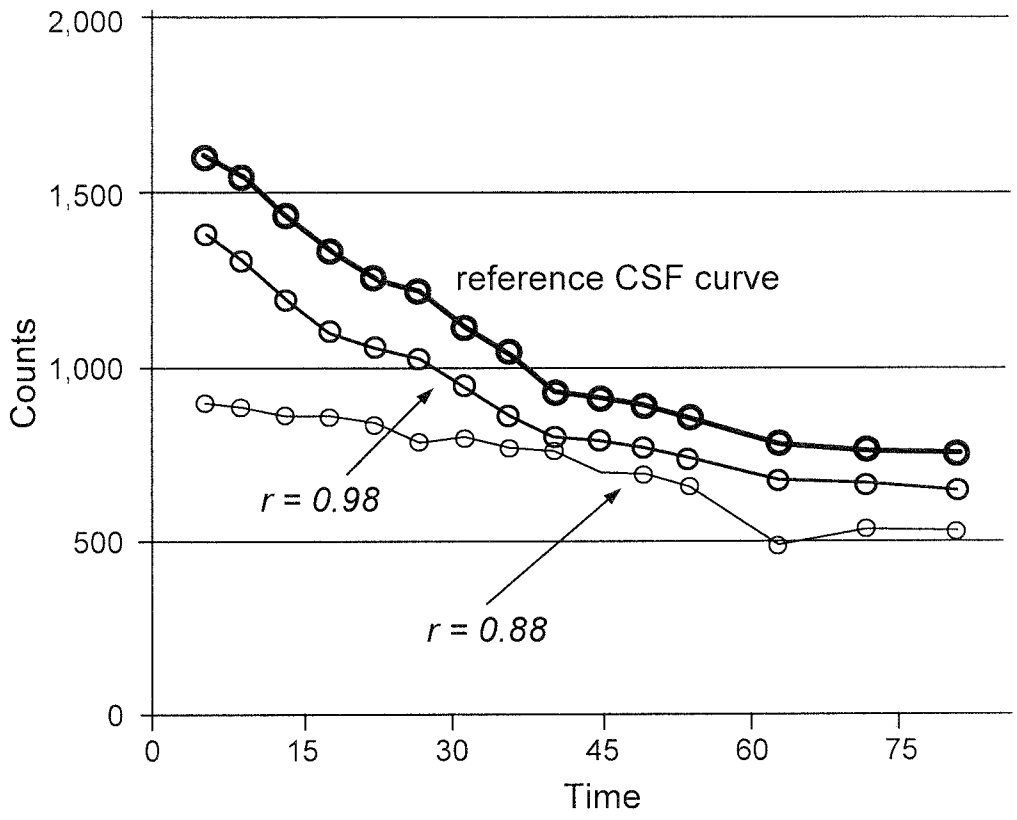
2,000
1,500
1,000
500
0
Counts
0
15
30
45
60
75
Time
reference CSF curve
r = 0.98
r = 0.88

Fig. 12

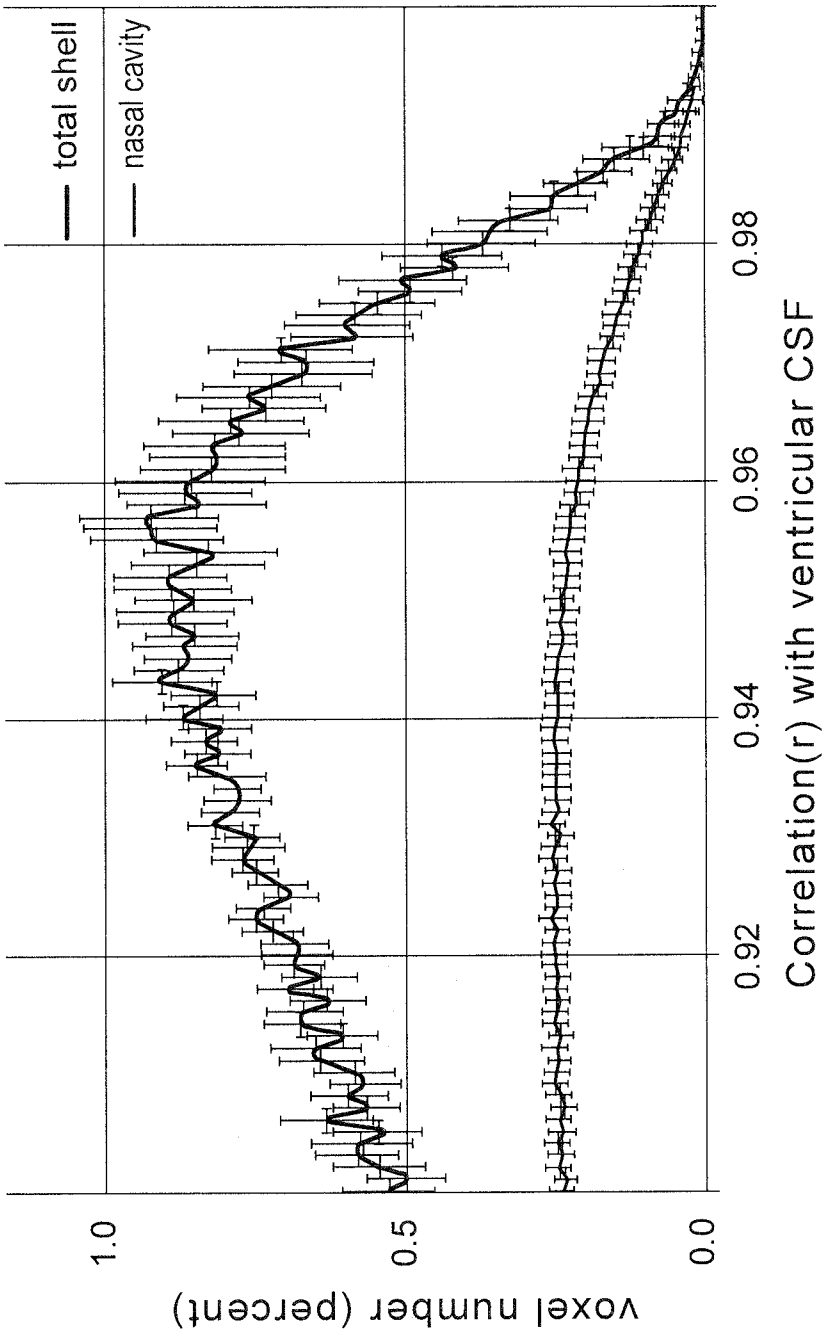
total shell
nasal cavity
1.0
0.5
0.0
voxel number (percent)
0.92
0.94
0.96
0.98
Correlation(r) with ventricular CSF

Fig. 13

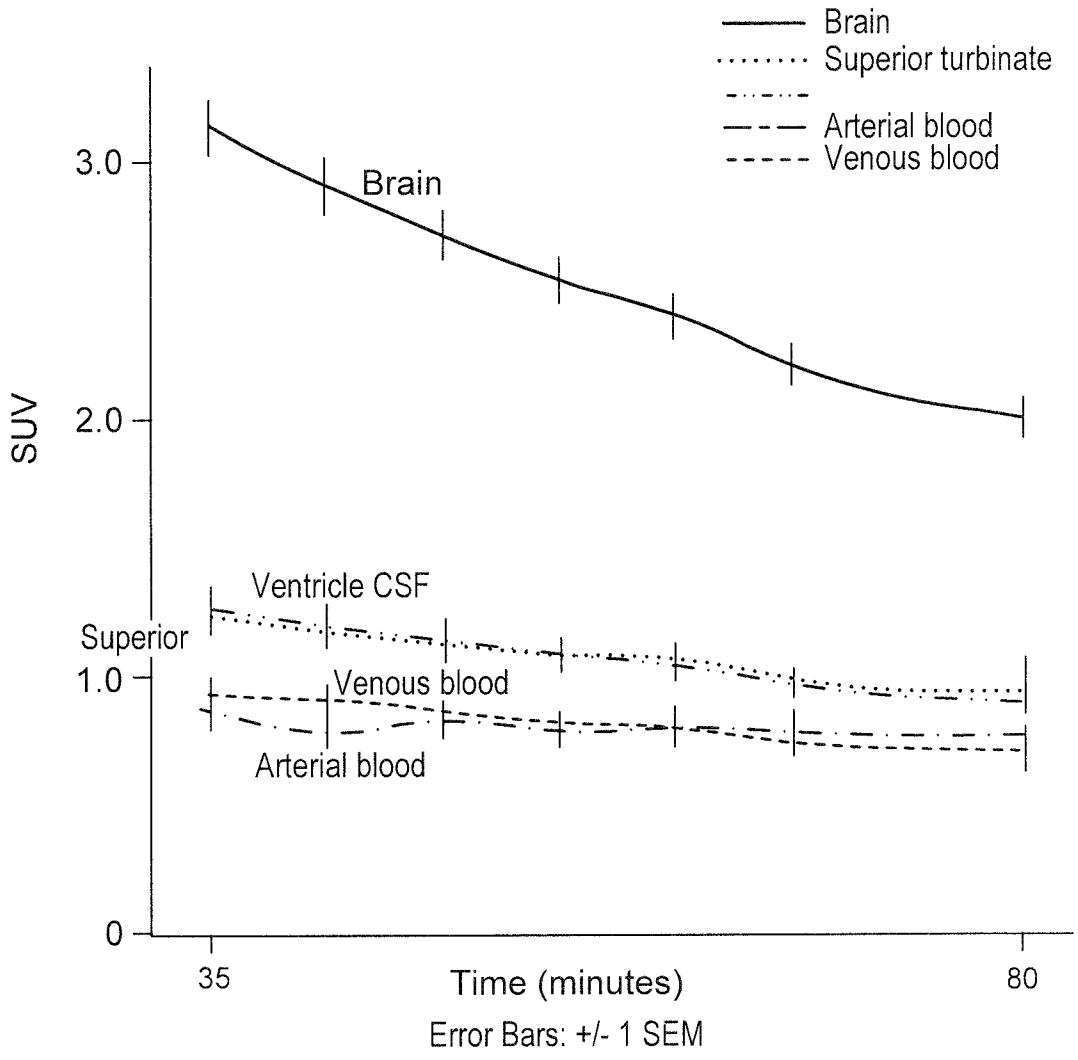
Brain
Superior turbinate
Arterial blood
Venous blood
3.0
2.0
1.0
0
SUV
Brain
Ventricle CSF
Superior
Venous blood
Arterial blood
35
Time (minutes)
80
Error Bars: +/- 1 SEM

Fig. 14

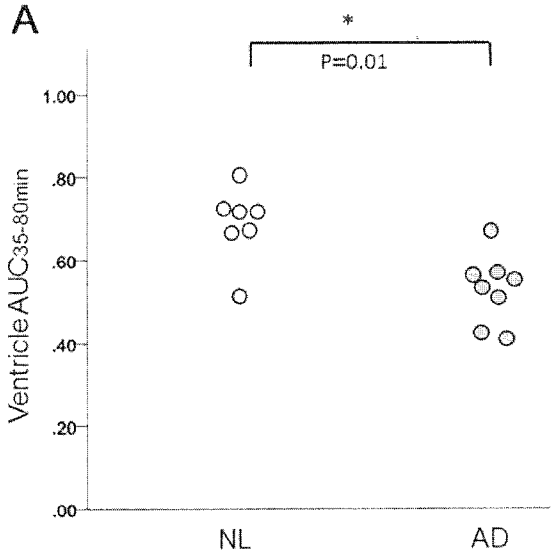

Fig. 15

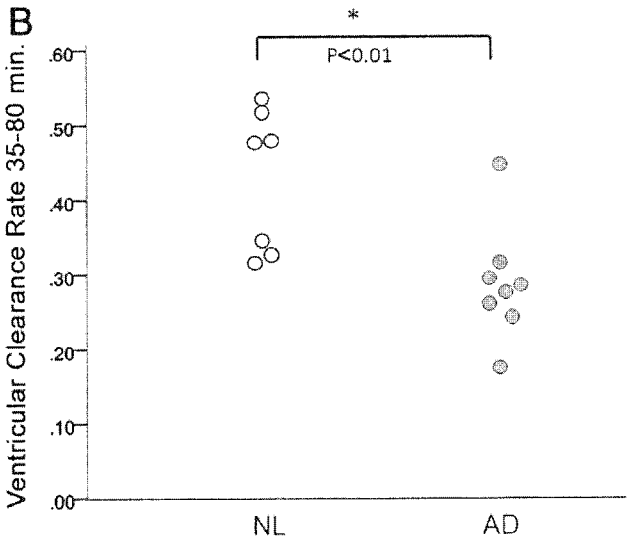

Fig. 16

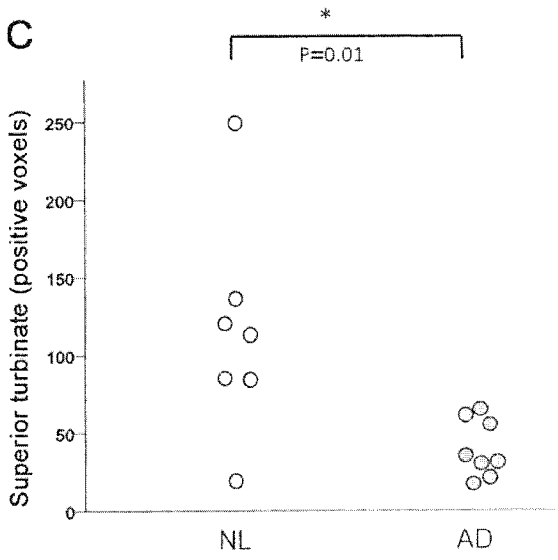

Fig. 17

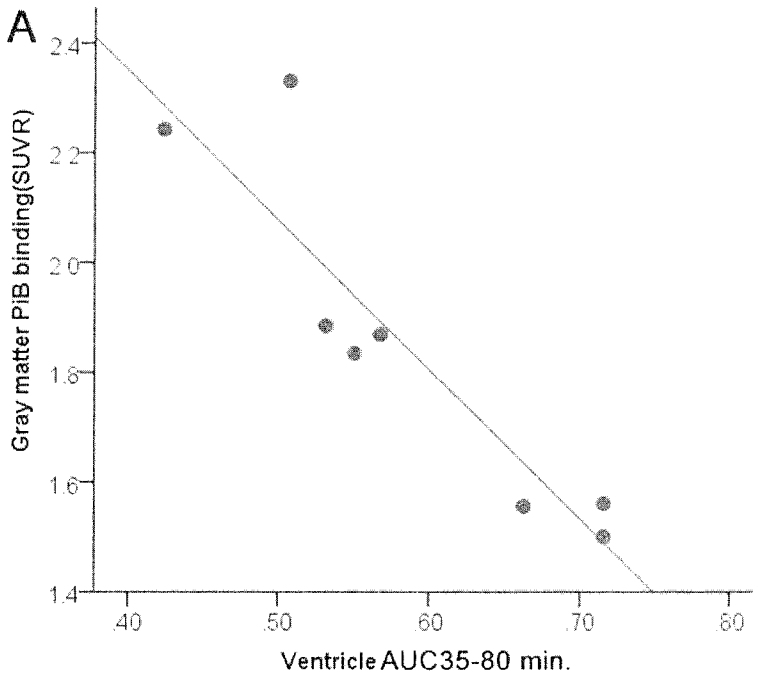
A
Gray matter PiB binding(SUVR)
2.4
2.2
2.0
1.8
1.6
1.4
.40
.50
.60
.70
.80
Ventricle AUC35-80 min.

Fig. 18

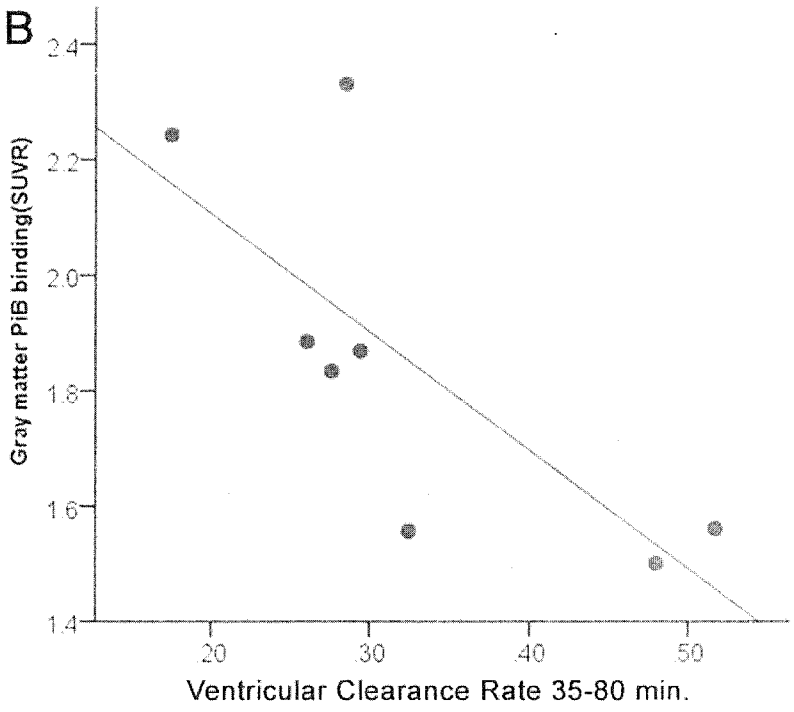
B
Gray matter PiB binding(SUVR)
2.4
2.2
2.0
1.8
1.6
1.4
.20
.30
.40
.50
Ventricular Clearance Rate 35-80 min.

Fig. 19

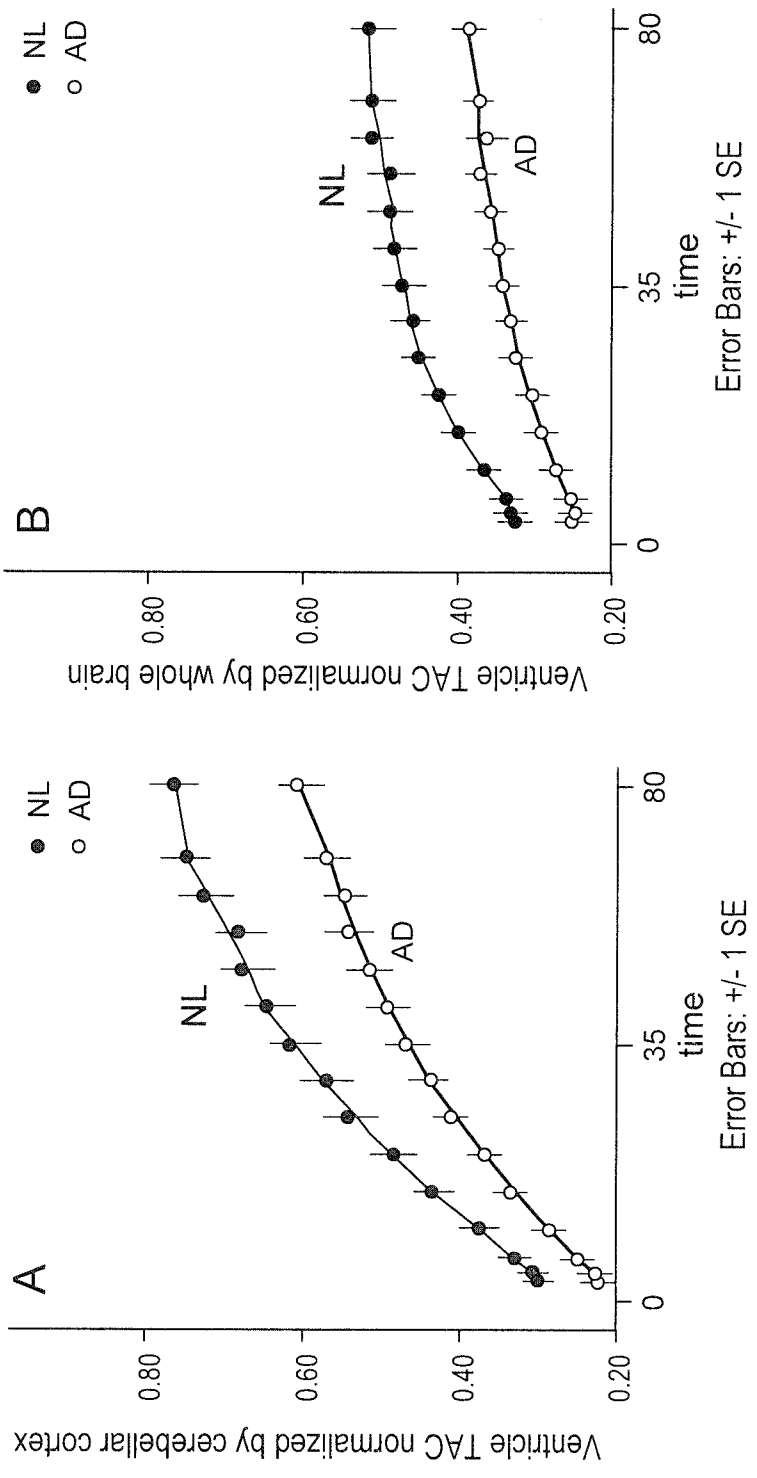
A
NL
AD
NL
AD
Ventricle TAC normalized by cerebellar cortex
0.20
0.40
0.60
0.80
0
35
80
time
Error Bars: +/- 1 SE
B
NL
AD
NL
AD
Ventricle TAC normalized by whole brain
0.20
0.40
0.60
0.80
0
35
80
time
Error Bars: +/- 1 SE

Fig. 20

Fig. 21

INTERNATIONAL SEARCH REPORT

International application No.
PCT/US2017/038342

A. CLASSIFICATION OF SUBJECT MATTER

IPC(8) - A61B 5/055; A61B 5/00; A61B 6/00; A61B 6/03; A61K 51/00; A61M 5/00; G01N 33/68 (2017.01)

CPC - G01R 33/5601; A61B 5/0037; A61B 5/055; A61B 5/40; A61B 5/4064; A61B 5/4076; A61B 5/4082; A61B 5/4088; A61B 6/037; A61B 2010/0077; A61B 2576/026; G01N 33/6896; G01N 2800/2821 (2017.08)

According to International Patent Classification (IPC) or to both national classification and IPC

B. FIELDS SEARCHED

Minimum documentation searched (classification system followed by classification symbols)

See Search History document

Documentation searched other than minimum documentation to the extent that such documents are included in the fields searched

USPC - 600/431; 382/128; 424/9.1; 424/9.3; 600/419 (keyword delimited)

Electronic data base consulted during the international search (name of data base and, where practicable, search terms used)

See Search History document

C. DOCUMENTS CONSIDERED TO BE RELEVANT

Category*	Citation of document, with indication, where appropriate, of the relevant passages	Relevant to claim No.
X	US 2016/0000945 A1 (UNIVERSITY OF ROCHESTER et al) 07 January 2016 (07.01.2016) entire document	1-21, 25-37
A	US 2007/0218002 A1 (BARRIO et al) 20 September 2007 (20.09.2007) entire document	1-37
A	US 2011/0166035 A1 (KLEINSCHMIDT et al) 07 July 2011 (07.07.2011) entire document	1-37
A	US 2014/0119621 A1 (UBER III) 01 May 2014 (01.05.2014) entire document	1-37

☐ Further documents are listed in the continuation of Box C. ☐ See patent family annex.

* Special categories of cited documents:

"A" document defining the general state of the art which is not considered to be of particular relevance

"E" earlier application or patent but published on or after the international filing date

"L" document which may throw doubts on priority claim(s) or which is cited to establish the publication date of another citation or other special reason (as specified)

"O" document referring to an oral disclosure, use, exhibition or other means

"P" document published prior to the international filing date but later than the priority date claimed

"T" later document published after the international filing date or priority date and not in conflict with the application but cited to understand the principle or theory underlying the invention

"X" document of particular relevance; the claimed invention cannot be considered novel or cannot be considered to involve an inventive step when the document is taken alone

"Y" document of particular relevance; the claimed invention cannot be considered to involve an inventive step when the document is combined with one or more other such documents, such combination being obvious to a person skilled in the art

"&" document member of the same patent family

Date of the actual completion of the international search	Date of mailing of the international search report
04 August 2017	22 AUG 2017
Name and mailing address of the ISA/US Mail Stop PCT, Attn: ISA/US, Commissioner for Patents P.O. Box 1450, Alexandria, VA 22313-1450 Facsimile No. 571-273-8300	Authorized officer Blaine R. Copenheaver PCT Helpdesk: 571-272-4300 PCT OSP: 571-272-7774